HHS Public Access

Author manuscript

Cell Rep. Author manuscript; available in PMC 2023 February 21.

Published in final edited form as:

Cell Rep. 2023 January 31; 42(1): 112004. doi:10.1016/j.celrep.2023.112004.

Downregulation of oxidative stress-mediated glial innate immune response suppresses seizures in a fly epilepsy model

Krishna M. Nukala[1], **Anthony J. Lilienthal**[1], **Shu Hui Lye**[2], **Alexander G. Bassuk**[3,4,5], **Stanislava Chtarbanova**[2], **J. Robert Manak**[1,3,6,*]

[1]Department of Biology, University of Iowa, Iowa City, IA 52242, USA

[2]Department of Biological Sciences, University of Alabama, Tuscaloosa, AL 35487, USA

[3]Department of Pediatrics, University of Iowa and Carver College of Medicine, Iowa City, IA 52242, USA

[4]Department of Neurology, University of Iowa and Carver College of Medicine, Iowa City, IA 52242, USA

[5]The Iowa Neuroscience Institute, University of Iowa and Carver College of Medicine, Iowa City, IA 52242, USA

[6]Lead contact

SUMMARY

Previous work in our laboratory has shown that mutations in *prickle* (*pk*) cause myoclonic-like seizures and ataxia in *Drosophila*, similar to what is observed in humans carrying mutations in orthologous *PRICKLE* genes. Here, we show that *pk* mutant brains show elevated, sustained neuronal cell death that correlates with increasing seizure penetrance, as well as an upregulation of mitochondrial oxidative stress and innate immune response (IIR) genes. Moreover, flies exhibiting more robust seizures show increased levels of IIR-associated target gene expression suggesting they may be linked. Genetic knockdown in glia of either arm of the IIR (Immune Deficiency [Imd] or Toll) leads to a reduction in neuronal death, which in turn suppresses seizure activity, with oxidative stress acting upstream of IIR. These data provide direct genetic evidence that oxidative stress in combination with glial-mediated IIR leads to progression of an epilepsy disorder.

Graphical Abstract

*Correspondence: john-manak@uiowa.edu.

AUTHOR CONTRIBUTIONS

K.M.N. and J.R.M. designed the study, analyzed and interpreted the data, and wrote the manuscript; K.M.N. generated all data unless otherwise specified; A.J.L. contributed the ubiquitous, pan-glial and pan-neuronal rescue data; A.G.B. and S.C. contributed experimental ideas and discussions; S.H.L. and S.C. interpreted and contributed the BEB and paraffin sectioning data.

DECLARATION OF INTERESTS

The authors declare no competing interests.

SUPPLEMENTAL INFORMATION

Supplemental information can be found online at https://doi.org/10.1016/j.celrep.2023.112004.

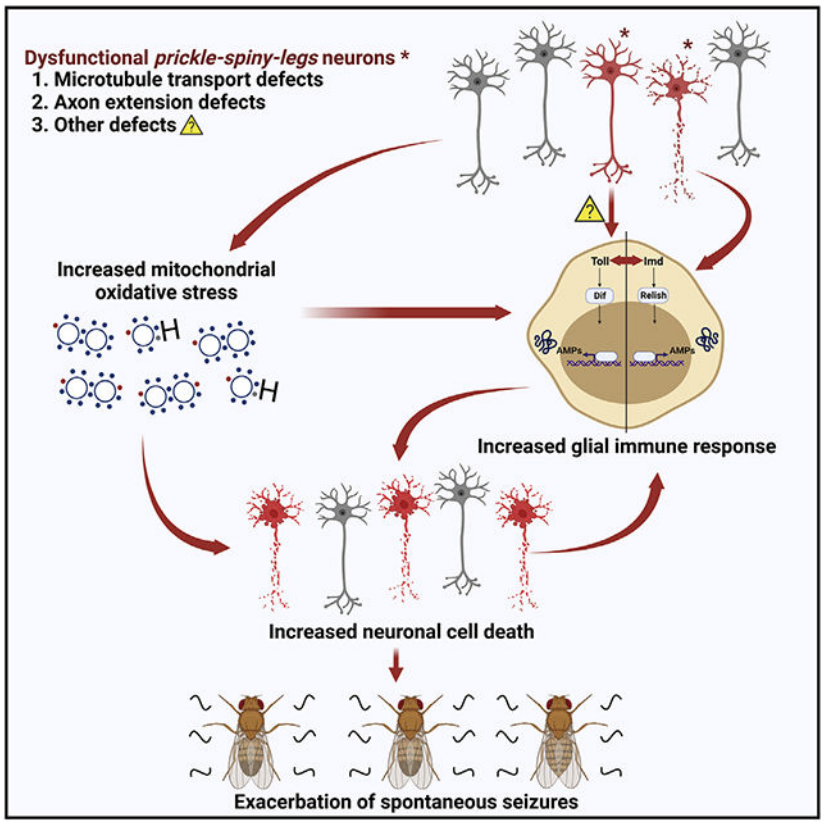

In brief

Although oxidative stress and immune system activation have been correlated with epilepsy, evidence for their direct involvement is lacking. Using a fly model of epilepsy, Nukala et al. genetically demonstrate that oxidative stress activates the glial innate immune response, which in turn contributes to progression of the epilepsy.

INTRODUCTION

Epilepsy, which affects ~1% of the US population, is a neurological disorder characterized by recurrent seizures leading to a significant impact on the quality of life and loss of productivity.[1,2] Approximately one-third of epilepsy patients do not respond to currently available therapies, and two-thirds of patients have adverse side effects to the medications.[3,4] Proteins encoded by the *PRICKLE* family of genes are part of the planar cell polarity (PCP) pathway that regulate neuronal function via noncanonical Wnt signaling.[5-7] In humans, *PRICKLE* mutations lead to an early-onset myoclonus-epilepsy and ataxia syndrome that worsens with age,[8-10] and mutations in *PRICKLE* orthologs lead to an increase in seizure susceptibility in flies, fish, and mice,[11,12] as well as defects in migration of facial branchiomotor neurons in fish and mice[13,14] and axonal advance of neurons in flies.[5,6]

Drosophila has a single *prickle* gene expressing two adult isoforms, *prickle-prickle* (pk^{pk}) and *prickle-spiny-legs* (pk^{sple}).[15] *prickle* is widely expressed in the developing fly brain,[11] and whereas homozygous loss-of-function (LOF) mutations in pk^{pk} result in

reduced viability,[16] homozygous LOF mutations in *pk*^{sple} lead to unprovoked, spontaneous myoclonus-like seizure activity and ataxia remarkably similar to those seen in human patients.[17] Finally, motor neurons in *pk*^{sple} mutants display enhanced anterograde vesicle transport in axons, and diminution of the transport by reducing the dosage of Kinesin anterograde motor protein subunits suppresses the seizures,[16] as does treatment with common human anti-epileptic drugs.[17]

The innate immune system is the first line of defense against pathogens, whereas the adaptive immune system makes use of immunological pathogen memory to combat further infections.[18] These two immune systems are intertwined and utilize a substantial amount of crosstalk to collaborate in fighting infection.[19,20] *Drosophila melanogaster* exclusively relies on an innate immune system,[21] providing a unique opportunity for specifically dissecting its role in neurological pathologies.[22] Two major nuclear factor κB (NF-κB) innate immune response (IIR) pathways exist in *Drosophila* (Toll and Immune Deficiency [Imd]), which are homologous to the mammalian Toll-like receptor (TLR) and tumor necrosis factor alpha (TNF-α) receptor (TNFR) pathways, respectively.[23] Activation of the Imd pathway leads to nuclear translocation of the NF-κB homolog Relish (Rel), which induces the expression of downstream targets, including anti-microbial peptide (AMP) genes.[24] Overexpression of *Rel* and AMPs has been linked to reduced lifespan, locomotor defects, and neurodegeneration in multiple fly disease models, including ataxia telangiectasia,[25,26] Parkinson's disease,[27] and traumatic brain injury (TBI),[28-30] whereas knockdown of *Rel* especially in glial cells has been shown to significantly increase lifespan while reducing neurodegeneration and locomotor defects.[31,32]

Besides its primary function in protecting organisms from invading pathogens, the role of the innate immune system in epileptogenesis has been a topic of interest in recent years.[33,34] In vertebrates, components of the interleukin-1 receptor (IL-1R)/TLR signaling pathway play a pivotal role in neuronal hyperexcitability through rapid post-translational changes in neuronal channels and neurotransmitter receptors, specifically *N*-methyl-D-aspartate (NMDA) receptors,[35-37] and TLR4-defective mice are resistant to kainate-induced seizures.[36] Studies have also noted prominent expression of IL-1β and TNF-α in astrocytes and activated microglia of both rodents and human patients with chronic epilepsy,[38-40] while induction of the TNF-α pathway by activated microglia promotes neuronal hyperexcitability through excessive release of glutamate by astrocytes.[41] Moreover, activation of both pro-inflammatory cyclooxygenases and the membrane attack pathway of the IIR-associated complement system has been linked to decreased seizure threshold and cell death in multiple models of epilepsy.[42,43] Inhibition of the IL-1/TLR signaling pathway has been shown to significantly cut down seizure recurrence in mice,[44] and small-molecule inhibitors of neuroinflammation, such as Minozac[45] and minocycline,[46] have proven effective in alleviating early-life seizures, with minocycline also decreasing the susceptibility to a second seizure. Overall, these studies indicate that glial cells play a key role in IIR in the brain and suggest that activated microglia might play a role in neuroinflammation-mediated seizure exacerbation.

Although a great deal of evidence supports the role of glial-mediated neuroinflammation in seizure exacerbation, no genetic studies have directly connected activation of the IIR in glia

to seizure generation. Although microglial genetic ablation of *Tuberous Sclerosis Complex 1* (*TSC1*) was shown to activate the microglia, thereby leading to epileptogenesis, seizure generation occurred through an apparent inflammation-independent pathway.[47] Moreover, it has been reported that the mouse line used to target the Cre recombinase to microglia expresses Cre at an earlier time point in neuronal populations,[48] thereby complicating interpretations regarding glial-specific functions. Indeed, use of a conditional inactivation strategy to more precisely target deletion of *TSC1* to glia did not lead to spontaneous seizures in the mice,[49] arguing that glial mammalian target of rapamycin (mTOR) activation is not associated with epileptogenesis per se.

In this study, we identify oxidative stress and IIR components to seizure exacerbation in our *Drosophila* model of a human epilepsy syndrome. We report that homozygous pk^{sple} mutant brains show an increase in oxidative stress, IIR, and neuronal cell death that correlates with seizure penetrance. Through glial-specific suppression of the IIR, we show that the increased neuronal cell death can be suppressed, which in turn suppresses the seizure exacerbation, and that mitigating oxidative stress in the pk^{sple} mutant nervous system suppresses both the neuronal cell death and seizure progression in part by reducing the IIR. These data establish a direct genetic connection between an increase in oxidative stress and glial-derived IIR and exacerbation of pk^{sple}-mediated epileptic seizures.

RESULTS

Expression of pk^{sple} only in neurons is sufficient to prevent seizures in pk^{sple} mutants

In order to determine whether the unprovoked, spontaneous seizures previously reported for homozygous pk^{sple} mutants[11,17] are the result of neuronal dysfunction, we used the Galactose responsive transcription factor 4/Upstream Activation Sequence (Gal4/UAS) expression system[50] to drive pk^{sple} in the entire organism, neurons, or glial cells of pk^{sple} mutants and then quantified spontaneous seizure activity.[17] As shown in Figure 1, seizure activity for both male and female pk^{sple} mutants was suppressed when pk^{sple} was expressed in the entire organism ($p < 0.0001$; Figure 1A; see Data S1 for p values of all pairwise data comparisons), as well as specifically in neurons ($p < 0.0001$; Figure 1B), but not when expressed in glial cells ($p > 0.05$; Figure 1C), thus indicating that seizures in pk^{sple} mutants are neuronally derived. Although both pk^{sple} mutant males and females showed strongly significant seizure activity, pk^{sple} mutant males routinely had more robust seizures than females (Table S1).

IIR genes are upregulated in pk^{sple} mutant brains, correlating with seizure penetrance

Axonal extension defects are observed in pk^{sple} mutants,[5] and previous work in our laboratory identified enhanced anterograde axonal transport in pk^{sple} mutants,[16] indicating that pk^{sple} neurons are dysfunctional. To search for potential clues that might explain this dysfunction, we performed a microarray and Gene Ontology (GO) analysis on 7- to 10-day-old homozygous pk^{sple} mutant brains compared with controls to identify dysregulated gene pathways (Figure 2A). Given that some gene expression changes might be specific to subsets of neuronal populations, we chose more moderate fold-change cutoffs (>1.5, <0.66) and identified a total of 960 significantly differentially expressed genes (adjusted $p < 0.05$;

444 upregulated, 516 downregulated; GEO: GSE154686). The Database for Annotation, Visualization, and Integrated Discovery (DAVID) functional annotation bioinformatics tool[51-53] was then used to identify GO pathways enriched in our dataset (see Data S2 for enrichment scores). We identified categories of genes connected to IIR, oxidation-reduction, flavonoid biosynthesis, and heat shock response, with the highest GO enrichment score associated with IIR (3.73; Figure 2B). Among the upregulated genes in this group were eight encoding AMPs, including *Attacin A, Attacin C, Cecropin A1, Cecropin A2, Cecropin C, Drosocin, Metchnikowin*, and *Diptericin A*, and an immune peptide *IM18*.

A second GO class enriched in our dataset was oxidation-reduction pathway (enrichment score of 3.2; Figure 2B), for which we identified 41 genes (18 upregulated, 23 downregulated). Among the upregulated genes were those encoding mitochondrial NADH dehydrogenases, a catalase, an aldo-keto reductase, and cytochrome P450 enzymes, all of which have been implicated in combating oxidative stress by carrying out detoxification processes in the cell.[54-57] Two related enriched GO classes associated with oxidative stress and detoxification were flavonoid biosynthesis (enrichment score: 3.14; 10 genes upregulated; Figure 2B)[58] and glutathione-*S*-transferases (enrichment score 0.58; three genes upregulated, two downregulated).[59] Among the downregulated oxidation-reduction genes were Nox and Duox, NADPH and dual oxidases, respectively, which are known to be major sources of cellular reactive oxygen species (ROS).[60]

To confirm the upregulation of AMPs and *IM18* in brains of the pk^{sple} mutants, we quantified expression of individual AMP genes in control and pk^{sple} mutant brains using qRT-PCR (see Table S2 for primer sequences). We observed significant upregulation of all AMPs and *IM18* ($p < 0.05$; Figure 2C). To determine whether there is a correlation between AMP/*IM18* gene expression and seizure penetrance, we used qRT-PCR to quantify AMP and *IM18* expression levels in brains of 7–10 days posteclosion (dpe) pk^{sple} mutants separated based on seizure penetrance (high versus no seizures; see STAR Methods) along with controls. We found that for most AMP genes, expression was significantly higher in "high seizure" animals compared with controls and "no seizure" animals, whereas AMP gene expression was either downregulated or not significantly different in "no seizure" animals compared with controls (Figure 2D). These data suggest that IIR activation may play a role in seizure penetrance.

Next, we crossed *AMP*-GFP transcriptional reporters representing three of the upregulated AMPs (*Attacin A, Cecropin A*, and *Drosocin*) into pk^{sple} mutants and controls and performed immunohistochemistry (IHC) to visualize GFP expression in fly brains aged to 0, 5, 15, and 30 dpe (Figures 2E, S1A, and S1B). At 15 dpe, we observed a significant increase in the percentage of GFP puncta in the pk^{sple} mutant brains for *Attacin*-GFP, *Cecropin*-GFP, and *Drosocin*-GFP ($p < 0.05$). We observed a similar increase in GFP puncta in pk^{sple} mutant brains at 30 dpe for *Attacin*-GFP and *Cecropin*-GFP ($p < 0.01$), but not *Drosocin*-GFP, whereas at 0 and 5 dpe, we observed a significant increase in GFP puncta only in pk^{sple} mutant brains for *Attacin*-GFP ($p < 0.05$), but not *Cecropin*-GFP or *Drosocin*-GFP. We also assessed *Attacin*-GFP, *Cecropin*-GFP, and *Drosocin*-GFP expression in pk^{sple} mutant third instar larval brains but found no significant difference in any of the reporters compared with

controls (Figure S1C). Collectively, these data suggest that the robust activation of the IIR in *pk*^{sple} brains occurs in adults, but not larvae.

To test whether glia are the source of the *AMP*-GFP signals, similar to what has been previously observed in fly brains carrying mutations that affect neuronal function,[25,26,31] we performed IHC on homozygous *pk*^{sple}*;Attacin-GFP* mutant brains expressing mCherry specifically in glial cells and used antibodies against GFP, mCherry, and neuronal marker Elav. As shown in Figures 3A and 3B, a significant percentage of mCherry-positive glia also show GFP co-localization, whereas a small percentage of GFP puncta also co-localize with Elav ($p < 0.05$), indicating that the majority of Attacin-GFP puncta are expressed in the glia. To confirm that glia are the primary source of AMP activation, we knocked down expression of *Rel* specifically in the glial cells in *pk*^{sple} mutant brains and assayed for *Attacin*-GFP puncta. As shown in Figures 3C and 3D, we observed a significant reduction of puncta ($p < 0.05$; Figure 3E), indicating that the glia are responsible for the upregulation of AMPs in *pk*^{sple} mutant brains.

To further test whether the increase in the IIR in the *pk*^{sple} mutant brains is indeed glial derived and not due to immune cells or commensal microorganisms infiltrating the brain from the periphery, we utilized a microinjection assay to assess the integrity of the blood-eye barrier (BEB) as a proxy for blood-brain barrier (BBB) integrity[61] in *pk*^{sple} mutants compared with controls. In this assay, 10,000 molecular weight (MW) fluorescent dextran molecules injected into the thorax of a fly will be excluded from entering the eye if the BBB is intact, forming a fluorescent hemolymph exclusion line surrounding the retina; conversely, if the BBB is compromised, the eye will fluoresce. Notably, no significant increase in fluorescence was observed in the eye of any of the injected *pk*^{sple} mutants, comparable with controls (Figures S2A-S2E), demonstrating that the BEB and BBB permeability is not impacted by the *pk*^{sple} mutation, and that the IIR in *pk*^{sple} brains can be attributed to the brain glial cells. Collectively, these data demonstrate that *AMP* genes are upregulated across adulthood in *pk*^{sple} mutant brains, similar to what has been observed for other fly neurological mutants,[25-27,31] and that glial are the major source of AMP upregulation.

pk^{sple} mutants show evidence of sustained neuronal cell death and an increase in seizure activity with age

As flies age, the brain-derived innate immune system is dysregulated, leading to an upregulation of AMPs, which in turn causes an increase in neuronal cell death and shortened lifespan.[31] Given our observation that *pk*^{sple} mutants showed an increase in IIR, we thus assessed whether *pk*^{ple} mutant brains had elevated neuronal cell death. We observed a significant increase in the percentage of cleaved Dcp-1 puncta in *pk*^{sple} mutants for all time points examined compared with controls ($p < 0.001$; Figures 4A-4I). Indeed, quantification of immunohistochemical co-localization of the anti-cleaved Dcp-1, a marker for apoptotic cells, with either an antibody for the neuronal marker Elav or an antibody for the glial marker Repo, indicated evidence of significant neuronal cell death occurring in *pk*^{sple} mutant brains (Figures 4J-4L). However, paraffin sectioning followed by H&E staining of *pk*^{sple} brains (Figures S2F-S2I) did not reveal the presence of widespread vacuoles observed in

brains of other fly neurodegeneration mutants,[25-31] suggesting that the neuronal cell death in pk^{sple} mutants is not extensive enough to generate regions devoid of neuronal matter.

Given that post-embryonic *prickle* is primarily expressed in the larval CNS,[62] we quantified neuronal cell death in pk^{sple} mutant third instar larvae. IHC of third instar larval brains showed a significant increase in the percentage of cleaved Dcp-1 puncta in pk^{sple} mutants ($p < 0.001$), indicating that the sustained neuronal cell death occurring in pk^{sple} mutant brains extends back to the larval stage (Figures 4M and 4N).

Given the sustained neuronal cell death in pk^{sple} mutant brains, and the observation that seizures in humans carrying *PRICKLE* mutations start early in childhood and worsen with age,[10] we sought to determine whether seizures exhibited by pk^{sple} mutants also increased with age. We thus performed the spontaneous seizure assay[17] on pk^{sple} mutant flies aged to 0, 5, 15, and 30 dpe. As shown in Figure 4O, male pk^{sple} mutants exhibited a large increase in spontaneous seizure activity from 0 to 5 dpe, and a nearly 2-fold increase in spontaneous seizure activity from 5 to 15 dpe ($p < 0.0001$), whereas no significant increase was observed comparing 15 with 30 dpe. When we quantified spontaneous seizure activity among female pk^{sple} mutants, we observed an increase in seizure penetrance across all time points. In summary, pk^{sple} mutants show increased seizure penetrance and continual neuronal cell death as they age, potentially suggesting a link between the two.

Inhibiting apoptosis in pk^{sple} mutant neurons suppresses neuronal cell death and seizures

The results obtained so far prompted us to formulate the hypothesis that dysfunctional neurons in pk^{sple} mutants induce a glial-mediated IIR that leads to the increased neuronal cell death and exacerbation of seizures. To provide evidence for this model, we therefore assessed whether inhibiting neuronal cell death in pk^{sple} mutant neurons suppressed seizure exacerbation in pk^{sple} mutants. We used the Gal4/UAS system to drive expression of *Drosophila inhibitor of apoptosis 1* (*Diap1*, a known inhibitor of effector caspases[63,64]) specifically in neurons of pk^{sple} mutants, followed by aging the flies to 15 dpe and either staining the brains for cleaved Dcp-1 or subjecting the flies to the spontaneous seizure assay. As shown in Figures 5A, 5B, and S3A-S3E, we not only observed a significant reduction in neuronal cell death ($p < 0.0001$) but also a robust suppression of spontaneous seizure activity ($p < 0.0001$; also see Figure S4A). These results indicate that inhibiting neuronal cell death in the brains of pk^{sple} mutants leads to a suppression of seizure activity, thereby demonstrating that the sustained neurodegeneration observed in pk^{sple} mutants leads to the exacerbation of seizure activity.

Next, we decided to assess whether AMPs and *IM18* are still activated in the pk^{sple} mutants even when *Diap1* is overexpressed in neurons of pk^{sple} mutants. Interestingly, we observed that several AMPs, including *Attacin A, Attacin C, Drosocin, Metchnikowin*, *Cecropin C*, and *Diptericin*, are significantly downregulated on inhibition of neuronal apoptosis of pk^{sple} mutants ($p < 0.05$; Figure 5C), thereby suggesting that dying neurons in pk^{sple} mutant brains could be signaling to the glia to activate an IIR.

Knockdown of IIR in homozygous pk^{sple} mutants suppresses seizures

To test the most important aspect of our model, namely, that the IIR is the initiator of the observed neuronal cell death, which in turn exacerbates the seizures, we generated pk^{sple};Rel^{E20} double-homozygous mutants, aged them to 15 dpe, and assessed both neuronal cell death and seizure penetrance. Intriguingly, pk^{sple};Rel^{E20} double-homozygous mutants not only showed a significant drop in the mean percentage of cleaved Dcp-1 puncta in the brain compared with controls ($p < 0.0001$; Figures S5A-S5E) but also showed a reduction in spontaneous seizure events ($p < 0.01$; Figure S5F).

Because glia in the *Drosophila* brain are responsible for expressing AMPs, we used either a glia-specific (*repo*-Gal4) or a neuron-specific (*elav*-Gal4) Gal4 driver along with a UAS-*RelRNAi* construct (see Figures S4B and S4C for validation) to specifically ablate *Rel* in glia and neurons of pk^{sple} mutants, respectively, followed by assessing neuronal cell death and seizure penetrance at 15 dpe. Notably, glial-specific knockdown of *Rel* in pk^{sple} mutants was sufficient to significantly reduce neuronal cell death ($p < 0.0001$) and suppress seizure penetrance ($p < 0.0001$; Figures 5D, 5E, and S3F-S3J), whereas knockdown of *Rel* in neurons showed no significant suppression in seizures (Figure S5G; also see Figure S4A). Additionally, qRT-PCR of AMPs and *IM18* isolated from brains of the glial *Rel* knockdown in pk^{sple} mutants compared with controls revealed that several AMP genes are significantly downregulated, including *Attacin A, Attacin C, Drosocin, Metchnikowin, Cecropin C*, and *Diptericin* ($p < 0.05$; Figure 5F).

We also tested whether the other arm of the innate immune system, the Toll pathway, might also be involved in increased neuronal cell death and exacerbation of seizures in pk^{sple} mutants. Because the NF-κB transcription factor Dorsal-related immunity factor (Dif) plays a key role in regulating IIR genes in this pathway,[21,23,65-68] we used a UAS-*DifRNAi* construct (see Figures S4D and S4E for validation) in combination with *repo*-Gal4 to knock down *Dif* expression in glial cells of the pk^{sple} mutants. Similar to what we observed for knockdown of the Imd pathway, glial-specific knockdown of *Dif* was able to significantly suppress both the increase in neuronal cell death ($p < 0.0001$) and the exacerbation of seizures ($p < 0.0001$; Figures 5G, 5H, and S3K-S3O). Additionally, qRT-PCR of AMPs and *IM18* isolated from brains of the glial *Dif* knockdown in pk^{sple} mutants compared with controls revealed that several AMP genes were significantly downregulated, including *Attacin A, Attacin C, Drosocin*, and *Metchnikowin* ($p < 0.05$; Figure 5I). Interestingly, we observed that several AMPs (*Attacin A, Attacin C, Drosocin*, and *Metchnikowin*) are significantly downregulated when either *Rel* or *Dif* is knocked down in glia, whereas *Cecropin C* and *Diptericin* are significantly downregulated only when *Rel* is knocked down ($p < 0.05$), demonstrating that both *Rel* and *Dif* coregulate some of the same AMPs in the brain. Collectively, these results demonstrate that dysfunctional neurons of homozygous pk^{sple} mutants lead to an increase in the glial-derived IIR, thus promoting an increase in neuronal cell death that in turn exacerbates the seizure phenotype, establishing a direct causal relationship between innate immune system activation and epilepsy severity.

Increased oxidative stress in *pk^{sple}* mutant neurons contributes to IIR upregulation, neuronal cell death, and exacerbation of seizures

Given the tightly correlated connections between oxidative stress and epilepsy,[69-74] and the significant increase in expression of genes involved in combating excessive oxidative stress in the *pk^{sple}* mutant brains (Figure 2B), we sought to determine whether *pk^{sple}* mutant brains showed increased oxidative stress. We thus assessed the presence of mitochondrial hydrogen peroxide in third instar larval and adult brains of *pk^{sple}* mutants and controls (0 and 5 dpe) using an *in vivo* ROS sensor (UAS-mt-roGFP2-Orp1).[75] Driving expression exclusively in neurons, we observed a significant increase in fluorescence intensity in *pk^{sple}* mutant third instar larval brains ($p < 0.01$), but no overall increase at 0 dpe ($p > 0.05$) and a significant decrease at 5 dpe ($p < 0.01$; Figures 6A-6I). Interestingly, the increased fluorescence in the larvae was located in optic lobe regions and primary/secondary neurons of the central brain region that will contribute to motor centers of the adult brain[76] (Figures 6A and 6B). In contrast, driving the sensor exclusively in glia revealed that glial-generated oxidative stress was actually lower in *pk^{sple}* larvae compared with controls ($p < 0.05$), but unchanged in both 0 and 5 dpe adult brains (Figures S6A-S6C). Collectively, these data indicate that neurons are the source of the increased oxidative stress in *pk^{sple}* mutants, and that there is a redistribution of oxidative stress signals occurring in the mutant brains compared with controls. Additionally, the increase in mitochondrial hydrogen peroxide, but not *AMP*-GFP expression, in third instar *pk^{sple}* mutant larval brains shows that increases in oxidative stress precede IIR activation.

To determine whether the increase in neuronal oxidative stress is contributing to an increase in neuronal cell death and exacerbation of seizures, we overexpressed *Superoxide dismutase 1* (*Sod1; UAS-Sod1*[77]), an ROS scavenger gene,[78] pan-neuronally using the Gal4/UAS system and assessed the downstream effects on cell death and seizures. As shown in Figures 6J, 6K, and S6D-S6H, pan-neuronal *Sod1* expression in *pk^{sple}* mutants significantly reduced the levels of both neuronal cell death and seizure exacerbation ($p < 0.05$). Next, we tested whether the increased oxidative stress in *pk^{sple}* mutant brains is upstream of the activation of glial immune response by quantifying the expression of AMP and *IM18* genes in *pk^{sple}* mutant brains overexpressing *Sod1* in neurons. As shown in Figure 6L, several AMPs, including *Attacin A, Attacin C, Drosocin, Metchnikowin*, and *Diptericin*, are significantly downregulated ($p < 0.05$) in *pk^{sple}* mutants overexpressing *Sod1*, indicating that oxidative stress can function upstream of the glial immune response.

DISCUSSION

Although our results support previous findings in rodent models of epilepsy whereby pharmacological inhibition of pro-inflammatory cytokines released by glial cells leads to seizure suppression,[44-46,79,80] we provide direct genetic evidence that specifically reducing the IIR in glia of an animal seizure model can suppress exacerbation of the seizure disorder. The use of a fly model allowed us to specifically assess the involvement of innate immune system activation in seizure generation, because unlike jawed vertebrates, flies do not utilize an adaptive immune system. Consistent with studies that have reported an IIR component associated with fly models of neurological diseases,[25-28] we show that IIR genes, including

those that encode AMPs, are robustly upregulated in pk^{sple} mutant brains (Figures 2A-2C), and we confirm that the source of the AMP activation is glia (Figure 3). We also show that there is a correlation between the levels of IIR gene expression and seizure robustness, suggesting a link between the two (Figure 2D). Next, we show that enhanced neuronal cell death in pk^{sple} mutant brains continues to accumulate as the flies age, during which time the seizure penetrance increases (Figure 4). Moreover, we show that glial-specific reduction of either arm of the IIR (Imd orToll) suppresses both the enhanced neuronal cell death and the seizure exacerbation, whereas expression of an anti-apoptosis factor specifically in neurons suppresses the seizure exacerbation, thus demonstrating a causal relationship between innate immune system activation, neurodegeneration, and seizure exacerbation (Figure 5). Finally, we show that neuronal oxidative stress is increased in pk^{sple} mutant brains prior to activation of the IIR, and that mitigation of the oxidative stress reduces the IIR, neuronal cell death, and seizure progression (Figure 6), thus supporting a model whereby increased oxidative stress promotes activation of the innate immune system, which leads to increased neuronal cell death followed by seizure exacerbation.

Previous work on pathogen-mediated IIR has revealed that Rel and Dif, in large part, activate independent sets of AMPs.[21,23,81-83] However, in the case of the glial-specific sterile inflammation that is observed in the pk^{sple} mutant brains, knockdown of either *Rel* or *Dif* results in suppression of many of the same AMPs, thus indicating that the two proteins collaborate to coregulate these genes in this context (Figures 5F and 5I).[84] Additionally, although *Cecropin A1*, *Cecropin A2*, and *IM18* are upregulated in pk^{sple} mutant brains, knockdown of either *Rel* or *Dif* fails to significantly reduce their expression, thus suggesting that one IIR pathway can compensate for loss of the other, or that these genes may be regulated by an alternative immune response/stress pathway.

How might oxidative stress lead to IIR activation? Mitochondrial oxidative stress in neurons leads to damage to mitochondrial membranes,[85] resulting in leakage of mitochondrial components, including mtDNA.[86] In vertebrates, cytosolic mtDNA leaked from dying or injured cells acts as damage-associated molecular patterns (DAMPS) to trigger an elevated immune response by directly engaging pattern-recognition receptors (PRRs).[87,88] Although this has not been demonstrated in mouse models of epilepsy, application of antioxidants such as *N*-acetylcysteine and sulforaphane in rat epilepsy models has been shown to delay the onset of epilepsy and reduce the frequency of seizures.[71] Additionally, several polyphenol compounds shown to reduce NF-κB signaling (and thus IIR) are known anti-oxidants,[89] raising the possibility that these compounds are exerting their effects through mitigation of oxidative stress, which in turn reduces the NF-κB-mediated IIR.

Although IIR activation via PRR recognition of DAMPs such as dsDNA has yet to be identified in flies,[90] the elevated mitochondrial oxidative stress we observe in the pk^{sple} larval brains results in downstream effects that trigger IIR activation, eventually leading to further neuronal cell death (Figure 6). Moreover, the process of cell death can also lead to an IIR (Figure 5). We hypothesize that the baseline neuronal dysfunction in pk^{sple} mutants (underscored by the axonal transport and oxidative stress defects) is likely the initial cause of neuronal cell death (via mitochondrial membrane disruption leading to apoptosis[72-74]) and perhaps seizure onset, and numerous studies have linked

axonal transport defects (specifically defects in mitochondrial transport) to increased ROS production and neurodegeneration.[91-93] We also hypothesize that this initial round of cell death stimulates the glial IIR via DAMPs/PRRs, which leads to further cell death in the seizure circuitry perhaps by killing partially or even normally functioning neurons of the circuit because of the heightened AMP expression by glia in their vicinity. The consequences are significant; namely, a robust increase in seizure progression that is underscored by the data in Figure 2D showing that AMP levels are significantly higher in the "high seizure" compared with "no seizure" pk^{sple} mutant flies. The data from Figure 5B provide additional support for this hypothesis, because preventing the loss of dysfunctional neurons by inhibiting apoptosis is sufficient to reduce both the apoptosis and spontaneous seizure events down to levels observed in controls ($p = 0.36$ comparing *+/+* versus *sple/sple;elav-Gal4/UAS-DIAP1* for the Dcp-1 assay and $p > 0.27$ comparing *+/+* versus *sple/sple;elav-Gal4/UAS-DIAP1* for both males and females for spontaneous seizure assay; see Data S3).

Our data suggest that pk^{sple} mutant brains exhibit oxidative stress that is associated with mitochondrial dysfunction, and mitochondrial oxidative stress has been shown to correlate with epileptogenesis.[69-71] Indeed, recurrent seizures in rodents induce production of ROS, resulting in increased mitochondrial membrane permeability and reduced seizure threshold.[72] It has also been shown that, after an initial seizure event, excessive ROS production and calcium overload lead to excitotoxicity and apoptotic cell death in multiple cortical cell layers of the brain, in turn leading to additional seizure events.[73,74] In the fly model of Friedrich's ataxia, a neurodegenerative disorder that includes motor dysfunction, enhanced anterograde transport of mitochondria in motor neurons leads to an accumulation of dysfunctional mitochondria at the nerve terminal.[92] We previously reported enhanced anterograde transport in motor neurons of pk^{sple} mutants,[16] and coupled with the evidence of mitochondrial oxidative stress, these data suggest that a similar dysfunction at nerve termini might be occurring in pk^{sple} mutants, although this hypothesis would need to be tested. Intriguingly, the mitochondrial hydrogen peroxide patterns in pk^{sple} mutants are different compared with controls, suggesting that the brain of a seizure-prone pk^{sple} mutant shows a reorganization of brain activity (at least with regard to generation of ROS) with heightened mitochondrial oxidative stress appearing in the optic lobes and central brain primary/secondary neurons of larvae that will give rise to adult motor centers (Figures 6A and 6B). However, although overall oxidative stress levels in the early pk^{sple} mutant adult brains (Figures 6D-6F) are comparable between the mutants and controls, the pk^{sple} mutants show a more widespread elevated oxidative stress pattern, consistent with our observation that the immunoreactivity patterns of both AMP-GFP and Dcp-1 are also widespread in pk^{sple} mutant brains (Figures 2E, 4A-4I, and S1).

Our data correlating increases in seizure robustness with higher levels of IIR gene activation (Figure 2D) are intriguing and suggest that different individual pk^{sple} mutant flies activate their IIRs to dramatically different extents, resulting in different seizure outcomes, thus perhaps helping to explain the IIR and cell death variability from fly to fly across our experiments. Interestingly, brains from pk^{sple} mutants that did not have any seizures over the assayed time window showed unchanged or reduced AMP expression compared with controls. The most likely explanation is that, although an overall increase in oxidative stress

is initially observed in pk^{sple} mutants (Figures 6A-6C), the resulting activation of oxidative stress mitigator genes is effective in contributing to an overall reduction of oxidative stress in the "no seizure" pk^{sple} mutants (Figures 6G-6I), which would be predicted to lead to a reduced IIR. It then follows that the damage caused by the oxidative stress in the "high seizure" flies succeeds in reaching a threshold beyond mitigation or repair, thereby leading to a robust IIR.

How does IIR activation ultimately cause the death of neurons? Evidence in the fly field specifically points to AMPs as the key neurotoxic agent. For example, mutation of the AMP gene *Metchnikowin* was not only shown to protect flies from early death following IIR activation after TBI but also reduced TBI-associated climbing deficits while increasing lifespan in the absence or presence of TBI.[94] Additionally, overexpression of a variety of AMPs in either glia or neurons has been shown to cause neurodegeneration, with expression from glia causing the greatest levels of neurodegeneration.[95] Along these lines, overexpression of AMPs either broadly or in the fat body induced cellular apoptosis in muscle or fat body in addition to eliciting depolarization of mitochondria, thus resulting in shortened lifespan.[96] These results prompted Badinloo and colleagues[96] to propose a model whereby AMPs may kill cells by targeting their mitochondria, thereby inducing membrane rupture via pore formation.[97,98] Such a model is consistent with the idea that mitochondria evolved from engulfed prokaryotes and may have retained some of their characteristics, thus making them an ideal cellular target for AMPs. Alternatively, AMPs might act as actual signaling molecules in order to exert their neurodegenerative/neuronal cell death effects through receptor (G-protein-coupled receptor/tyrosine kinase/ligand-gated ion channel-mediated autophagy or apoptosis.[99]

In this study, we present an additional example of neuronal cell death that is initiated by glia through use of an innate immune system-activated "neurotoxic factor," namely, AMPs. However, such a model is not specific to flies. In fact, activated microglia in mice were previously shown to convert astrocytes (a type of glial cell) into an A1 subtype that was capable of killing neurons.[100] Intriguingly, downstream targets of this microglial IIR include components of the vertebrate versions of Toll and Imd (as well as C1q, part of the complement cascade), thus leading to formation of the membrane attack complex, which acts in a similar fashion to AMPs to kill cells by creating pores in the membrane.[101] Whether C1q is a component of the "neurotoxic factor" described by Liddelow and colleagues[100] remains to be determined.

Limitations of the study

Although our data are generally consistent with a pathway whereby neuronal oxidative stress leads to an IIR, which in turn increases neuronal cell death, thus leading to increased seizure penetrance, it is undeniable that the seizure exacerbation pathway is considerably more complex. This is supported by our observation that inhibition of neuronal cell death leads to a decrease in IIR, thus in this context potentially placing cell death upstream of IIR. It is therefore likely that the different insults acting both in series and independently may ultimately lead to increased seizure penetrance. In this regard, oxidative stress could directly contribute to neuronal cell death completely independent of IIR, which could then lead to

increased seizure penetrance, and that increased cell death from the combination of oxidative stress and IIR could create a positive feedback loop to further stimulate the IIR. Additional experiments will aim to tease apart the multi-level involvement of these processes.

STAR★METHODS

RESOURCE AVAILABILITY

Lead contact—Further information and requests for resources, reagents and source data should be directed to and will be fulfilled by the lead contact, J. Robert Manak (john-manak@uiowa.edu).

Materials availability—This study did not generate new unique reagents.

Data and code availability

- Microarray gene expression data is available at the GEO database, accession number GEO: GSE154686. Source data generated in this study is available as Data S3. Requests for resources and reagents used in this study should be directed to the lead contact.
- This paper does not report original code.
- Any additional information required to reanalyze the data reported in this paper is available from the lead contact upon request.

EXPERIMENTAL MODEL AND SUBJECT DETAILS

All fly lines used in this study are described in the key resources table. For all experiments, unless specified, male and female flies (*Drosophila melanogaster*) were reared and aged to specific timepoints as per experimental requirements in a 25°C incubator on a 12 h light/dark cycle using standard cornmeal-molasses medium food. For histology and BBB assays, Nutri-Fly® Bloomington formulation food (Genesee Scientific, Cat #: 66-113) was used. No institutional permission was required to perform the experiments mentioned in this study.

METHOD DETAILS

Spontaneous seizure assay—The spontaneous seizure assay was performed as described in[17] with a few modifications. For qRT-PCR experiments, pk^{sple} mutant flies that experienced at least 6 seizure events during a 15 minute assay were categorized as having high seizures while the pk^{sple} mutant flies that did not experience any seizures during the assay were categorized as having no seizures. All the flies assayed were aged for 7–10 dpe (except when mentioned otherwise) and were separated by sex a day prior to when the assay was performed and allowed to acclimate in an environmentally controlled chamber (Chamber Temperature: 25°C, Relative Humidity: 60%) in which the assay was performed. All videos taken were subjected to a single blind analysis to avoid bias.

Immunohistochemistry and confocal microscopy—For all immunohistochemistry procedures, adult fly and 3rd instar larval brains were dissected in 1X PBS and fixed in 4% paraformaldehyde in 1X PBS for 40 min, washed 5 successive times, 10 min each, in 0.03%

PBS-Triton and incubated for 40 mins at room temperature in blocking solution (0.1% PBS-Triton-BSA). Next, samples were incubated overnight at 4°C with primary antibodies diluted in blocking solution. Samples were then washed 6 times, 10 min each, with 0.03% PBS-Triton followed by incubation for 40 mins at room temperature in blocking solution. Next, samples were incubated for 2 h at room temperature with secondary antibodies diluted in blocking solution. After 6 successive 10 min washes with 0.03% PBS-Triton, brains were mounted in Vectashield® with DAPI mounting medium (Vector Laboratories). Brains were analysed under Leica TCS SP5 confocal microscope using a 20X dry objective or a 63X water objective and images were acquired using Lecia's LAS AF software. The following primary antibodies were used: rabbit anti-Dcp1 (1:100) (Cell Signaling Technologies), Rat-Elav-7E8A10 anti-elav (1:200) was deposited to the DSHB by Rubin, G.M. (DSHB Hybridoma Product Rat-Elav-7E8A10 anti-elav), 8D12 anti-Repo (1:300) was deposited to the DSHB by Goodman, C. (DSHB Hybridoma Product 8D12 anti-Repo), rabbit anti-GFP (1:500) (Invitrogen) and mouse 3A11 anti-mCherry (1:500) was deposited to the DSHB by DSHB (DSHB Hybridoma Product DSHB-mCherry-3A11). The following secondary antibodies were used: Alexa Fluor® 488-conjugated goat anti-rabbit (1:200 for anti-Dcp1) (1:500 for anti-GFP) (Inivitrogen), Alexa Fluor® 568-conjugated goat anti-mouse (1:300 for anti-repo and 1:500 for anti-mCherry), Alexa Fluor® 568-conjugated goat anti rat (1:300 for anti-elav) (Invitrogen) and Alexa Fluor® 633-conjugated goat anti rat (1:300 for anti-elav) (Invitrogen).

***In vivo* ROS measurement—**Mitochondrial ROS levels in controls and homozygous*pk*^{sple} mutants were quantified using *UAS-mito-roGFP2-Orp1* reporter line.[75] 3rd instar larval, 0-day and 5-day old brains were dissected in 1X Live Cell Imaging Solution (Invitrogen™ catalogue# A14291DJ) and immediately imaged by excitation at 488 nm (reduced), with emission recorded at 510 nm. Live imaging was performed using a Leica TCS SP8 confocal microscope using a 20X dry objective and images were acquired using Lecia's LAS AF software.

Image processing and quantification—ImageJ[102] was used for quantification and image processing. 30–40 μm maximum projection images of the adult mid-brain and maximum projections of the entire 3rd instar larval brain were used to quantify the number of Dcp-1 positive puncta. Background noise was removed using background subtraction (rolling = 5) and Gaussian blur filter (sigma = 0.5–1) or despeckling. Next, the images were manually thresholded and the apoptotic puncta were counted.

For the *AMP*-GFP assays, the number of GFP puncta was quantified in 30 μm max projections of the adult mid-brain, for *Cecropin*-GFP and the optic lobe, for *Attacin*-GFP and *Drosocin*-GFP due to the high constitutive expression of GFP in the antennal lobes of both control and mutants. The background noise was removed using background subtraction (rolling = 5) and Gaussian blur filter (sigma = 1) or despeckling followed by manual thresholding before quantifying GFP puncta. For both Dcp-1 and AMP-GFP quantifications, puncta were defined as fluorescent particles greater than 0.2 micron^2 after background noise removal and thresholding using ImageJ's "Analyze Particles" tool.

For *in vivo* ROS sensor experiments, maximum projection images of the entire 3rd instar larval brains (minus the ventral nerve cord) and adult brains were used to quantify the GFP fluorescent intensity.

For Dcp-1, *AMP*-GFP assays and *in vivo* ROS sensor experiments, the number of Dcp-1 positive puncta, the GFP puncta and GFP intensity were assumed to be 100% in the control for normalization purposes.

Histology and neurodegeneration—Flies of indicated genotypes were collected at 0–3 or 0–4 days after eclosion and aged at 25°C for up to 5- (range 3–8 days), 15- (range 14–18 days) or 30- (range 26–32 days) day old. At the desired age, fly heads were severed using a razorblade and placed in Carnoy's fixative (100% Ethanol:chloroform:acetic acid at 6:3:1) over night at 4°C. The fixation solution was replaced with 70% Ethanol the next day and the head paraffin embedding procedure, head sectioning (at 5 μm) and hematoxylin and eosin (H&E) staining were followed as described in.[103] The presence of neurodegeneration was indicated by the appearance of holes in the brain neuropil and was scored blindly for each genotype using the 6-level (scale of 0,1,2,3,4 and 5) neurodegeneration index score as described in.[95] Images were acquired using a Camera-equipped Nikon Eclipse E100 light microscope using the Nikon NIS-Elements image acquisition software. Acquired images were next processed using Adobe Creative Cloud Photoshop software for proper orientation in respective figures.

Blood brain barrier assay—Blood eye barrier (BEB) integrity was used as a proxy to determine blood brain barrier (BBB) integrity.[61,104] 6–10 day-old female flies of each genotype were individually injected under CO_2-anesthesia with 69 nL of 50 mg/mL of 10,000 MW Alexa Fluor® 488-Dextran (Invitrogen™ catalogue # D22910) using a glass capillary (Drummond 3-000-203-G/X) mounted on a Nanoject II Auto nanoliter injector (Drummond Scientific). Injected flies were incubated for 2 h at 25°C, following which they were anesthetized on ice, and placed under a fluorescent stereoscope to score BBB integrity. The presence of a fluorescent hemolymph exclusion line or diffused eye fluorescence was used to score intact and disrupted BBB, respectively. Representative images of eyes were acquired using a DSLR camera mounted on the stereoscope.

Gene expression and gene ontology analysis—Flies were aged to 7–10 days before dissecting their brains for microarray gene expression analysis which was performed as described in.[105] Two biological replicates with 4 technical replicates were used to perform the gene expression analysis. Genes were considered differentially expressed if showing an FDR-adjusted p value of less than 0.05 and a fold change value of ≥ 1.5 (upregulated) or ≤0.66 (downregulated).

ForqRT-PCR of AMP genes, RNA from 7 to 10 day old 25–30 adult brains per biological replicate was isolated using RNAqueous-Micro Total RNA Isolation kit (Invitrogen) according to manufacturer's instructions. cDNA was prepared from 0.2–0.5 μg total RNA using the High-Capacity RNA to cDNA kit (Applied Biosystems). Samples were amplified using the PowerUp SYBR Green Master Mix (Applied Biosystems) and quantified using Applied Biosystems 7900HT and QuantStudio 7 Pro real-time PCR machines according

to the manufacturer's protocols. The primers for the AMP genes (Table S2) were ordered from Integrated DNA Technologies, Inc. and primers for RNAi lines validation (Table S2) were ordered from FlyprimerBank.[106] Mean Ct values of three technical replicates for each biological replicate were calculated after normalizing to the housekeeping gene *rp49*, followed by the mean of the biological replicates. Log_2 fold change values were calculated relative to control. Statistical significance was calculated using a two-tailed unpaired Student's t test and One-way ANOVA with post-hoc comparisons test.

Gene ontology analysis was performed using DAVID[51,52] by inputting the list of differentially expressed genes and a list of significantly enriched GO terms were obtained.

QUANTIFICATION AND STATISTICAL ANALYSIS

Statistical analysis was performed using Graphpad Prism 9. All data were assessed for Gaussian distribution using the Shapiro-Wilk's normality test and analyzed with a two-tailed unpaired Student's t test, Mann-Whitney U test, One-way ANOVA and Kruskal-Wallis test. Error bars for all data represent the mean ± SEM. Two-tailed p values of <0.05 were considered the cutoff for statistical significance.

Supplementary Material

Refer to Web version on PubMed Central for supplementary material.

ACKNOWLEDGMENTS

This work was supported by NIH grants R01NS098590 (to J.R.M. and A.G.B.) and P50HD103556 and UIDM/Tross Family grant (to A.G.B.). S.C. was supported by start-up funds from the University of Alabama. We thank Courtney Schmitt and Cassidy Suther for seizure assay analysis and brain dissections.

REFERENCES

1. Frankel WN (2009). Genetics of complex neurological disease: challenges and opportunities for modeling epilepsy in mice and rats. Trends Genet. 25, 361–367. [PubMed: 19665252]
2. Kobau R, Price PH, Giles HW, Pennell PB, and Hargis E (2010). Centers for disease control and prevention managing epilepsy well network. Epilepsy Behav. 19, 216–217. [PubMed: 20933476]
3. Kwan P, and Brodie MJ (2000). Early identification of refractory epilepsy. N. Engl. J. Med 342, 314–319. [PubMed: 10660394]
4. Veeman MT, Axelrod JD, and Moon RT (2003). A second canon. Functions and mechanisms of beta-catenin-independent Wnt signaling. Dev. Cell 5, 367–377. [PubMed: 12967557]
5. Shimizu K, Sato M, and Tabata T (2011). The Wnt5/planar cell polarity pathway regulates axonal development of the Drosophila mushroom body neuron. J. Neurosci 31, 4944–4954. [PubMed: 21451033]
6. Mrkusich EM, Flanagan DJ, and Whitington PM (2011). The core planar cell polarity gene prickle interacts with flamingo to promote sensory axon advance in the Drosophila embryo. Dev. Biol 358, 224–230. [PubMed: 21827745]
7. Wada H, and Okamoto H (2009). Roles of planar cell polarity pathway genes for neural migration and differentiation. Dev. Growth Differ 51, 233–240. [PubMed: 19298553]
8. Tree DRP, Shulman JM, Rousset R, Scott MP, Gubb D, and Axelrod JD (2002). Prickle mediates feedback amplification to generate asymmetric planar cell polarity signaling. Cell 109, 371–381. [PubMed: 12015986]

9. Carreira-Barbosa F, Concha ML, Takeuchi M, Ueno N, Wilson SW, and Tada M (2003). Prickle 1 regulates cell movements during gastrulation and neuronal migration in zebrafish. Development 130, 4037–4046. [PubMed: 12874125]
10. Bassuk AG, Wallace RH, Buhr A, Buller AR, Afawi Z, Shimojo M, Miyata S, Chen S, Gonzalez-Alegre P, Griesbach HL, et al. (2008).A homozygous mutation in human PRICKLE1 causes an autosomal-recessive progressive myoclonus epilepsy-ataxia syndrome. Am. J. Hum. Genet 83, 572–581. [PubMed: 18976727]
11. Tao H, Manak JR, Sowers L, Mei X, Kiyonari H, Abe T, Dahdaleh NS, Yang T, Wu S, Chen S, et al. (2011). Mutations in prickle orthologs cause seizures in flies, mice, and humans. Am. J. Hum. Genet 88, 138–149. [PubMed: 21276947]
12. Mei X, Wu S, Bassuk AG, and Slusarski DC (2013). Mechanisms of prickle1a function in zebrafish epilepsy and retinal neurogenesis. Dis. Model. Mech 6, 679–688. [PubMed: 23324328]
13. Mapp OM, Walsh GS, Moens CB, Tada M, and Prince VE (2011). Zebrafish Prickle1b mediates facial branchiomotor neuron migration via a farnesylation-dependent nuclear activity. Development 138, 2121–2132. [PubMed: 21521740]
14. Yang T, Bassuk AG, Stricker S, and Fritzsch B (2014). Prickle1 is necessary for the caudal migration of murine facial branchiomotor neurons. Cell Tissue Res. 357, 549–561. [PubMed: 24927917]
15. Gubb D, Green C, Huen D, Coulson D, Johnson G, Tree D, Collier S, and Roote J (1999). The balance between isoforms of the Prickle LIM domain protein is critical for planar polarity in Drosophila imaginal discs. Genes Dev. 13, 2315–2327. [PubMed: 10485852]
16. Ehaideb SN, Iyengar A, Ueda A, Iacobucci GJ, Cranston C, Bassuk AG, Gubb D, Axelrod JD, Gunawardena S, Wu CF, and Manak JR (2014). Prickle modulates microtubule polarity and axonal transport to ameliorate seizures in flies. Proc. Natl. Acad. Sci. USA 111, 11187–11192. [PubMed: 25024231]
17. Ehaideb SN, Wignall EA, Kasuya J, Evans WH, Iyengar A, Koerselman HL, Lilienthal AJ, Bassuk AG, Kitamoto T, and Manak JR (2016). Mutation of orthologous prickle genes causes a similar epilepsy syndrome in flies and humans. Ann. Clin. Transl. Neurol 3, 695–707. [PubMed: 27648459]
18. Smith NC, Rise ML, and Christian SL (2019). A comparison of the innate and adaptive immune systems in cartilaginous fish, ray-finned fish, and lobe-finned fish. Front. Immunol 10, 2292. [PubMed: 31649660]
19. Clark R, and Kupper T (2005). Old meets new: the interaction between innate and adaptive immunity. J. Invest. Dermatol 125, 629–637. [PubMed: 16185260]
20. Getz GS (2005). Thematic review series: the immune system and atherogenesis. Bridging the innate and adaptive immune systems. J. Lipid Res 46, 619–622. [PubMed: 15722562]
21. Hoffmann JA (2003). The immune response of Drosophila. Nature 426, 33–38. [PubMed: 14603309]
22. Hoffmann JA, and Reichhart JM (2002). Drosophila innate immunity: an evolutionary perspective. Nat. Immunol 3, 121–126. [PubMed: 11812988]
23. Lemaitre B, and Hoffmann J (2007). The host defense of Drosophila melanogaster. Annu. Rev. Immunol 25, 697–743. [PubMed: 17201680]
24. Stoven S, Silverman N, Junell A, Hedengren-Olcott M, Erturk D, Engstrom Y, Maniatis T, and Hultmark D (2003). Caspase-mediated processing of the Drosophila NF-kappaB factor Relish. Proc. Natl. Acad. Sci. USA 100, 5991–5996. [PubMed: 12732719]
25. Petersen AJ, Katzenberger RJ, and Wassarman DA (2013). The innate immune response transcription factor relish is necessary for neurodegeneration in a Drosophila model of ataxia-telangiectasia. Genetics 194, 133–142. [PubMed: 23502677]
26. Petersen AJ, Rimkus SA, and Wassarman DA (2012). ATM kinase inhibition in glial cells activates the innate immune response and causes neurodegeneration in Drosophila. Proc. Natl. Acad. Sci. USA 109, E656–E664. [PubMed: 22355133]
27. Maitra U, Scaglione MN, Chtarbanova S, and O'Donnell JM (2019). Innate immune responses to paraquat exposure in a Drosophila model of Parkinson's disease. Sci. Rep 9, 12714. [PubMed: 31481676]

28. Katzenberger RJ, Loewen CA, Wassarman DR, Petersen AJ, Ganetzky B, and Wassarman DA (2013). A Drosophila model of closed head traumatic brain injury. Proc. Natl. Acad. Sci. USA 110, E4152–E4159. [PubMed: 24127584]
29. Katzenberger RJ, Chtarbanova S, Rimkus SA, Fischer JA, Kaur G, Seppala JM, Swanson LC, Zajac JE, Ganetzky B, and Wassarman DA (2015). Death following traumatic brain injury in Drosophila is associated with intestinal barrier dysfunction. Elife 4, e04790. [PubMed: 25742603]
30. Katzenberger RJ, Ganetzky B, and Wassarman DA (2015). The gut reaction to traumatic brain injury. Fly 9, 68–74. [PubMed: 26291482]
31. Kounatidis I, Chtarbanova S, Cao Y, Hayne M, Jayanth D, Ganetzky B, and Ligoxygakis P (2017). NF-kappaB immunity in the brain determines fly lifespan in healthy aging and age-related neurodegeneration. Cell Rep. 19, 836–848. [PubMed: 28445733]
32. Tan L, Schedl P, Song HJ, Garza D, and Konsolaki M (2008). The Toll->NFkappaB signaling pathway mediates the neuropathological effects of the human Alzheimer's Abeta42 polypeptide in Drosophila. PLoS One 3, e3966. [PubMed: 19088848]
33. Vezzani A, French J, Bartfai T, and Baram TZ (2011). The role of inflammation in epilepsy. Nat. Rev. Neurol 7, 31–40. [PubMed: 21135885]
34. Vezzani A, Friedman A, and Dingledine RJ (2013). The role of inflammation in epileptogenesis. Neuropharmacology 69, 16–24. [PubMed: 22521336]
35. Balosso S, Maroso M, Sanchez-Alavez M, Ravizza T, Frasca A, Bartfai T, and Vezzani A (2008). A novel non-transcriptional pathway mediates the proconvulsive effects of interleukin-1beta. Brain 131, 3256–3265. [PubMed: 18952671]
36. Maroso M, Balosso S, Ravizza T, Liu J, Aronica E, Iyer AM, Rossetti C, Molteni M, Casalgrandi M, Manfredi AA, et al. (2010). Toll-like receptor 4 and high-mobility group box-1 are involved in ictogenesis and can be targeted to reduce seizures. Nat. Med 16, 413–419. [PubMed: 20348922]
37. Viviani B, Bartesaghi S, Gardoni F, Vezzani A, Behrens MM, Bartfai T, Binaglia M, Corsini E, Di Luca M, Galli CL, and Marinovich M (2003). Interleukin-1beta enhances NMDA receptor-mediated intracellular calcium increase through activation of the Src family of kinases. J. Neurosci 23, 8692–8700. [PubMed: 14507968]
38. Ravizza T, Gagliardi B, Noé F, Boer K, Aronica E, and Vezzani A (2008). Innate and adaptive immunity during epileptogenesis and spontaneous seizures: evidence from experimental models and human temporal lobe epilepsy. Neurobiol. Dis 29, 142–160. [PubMed: 17931873]
39. Balosso S, Ravizza T, Perego C, Peschon J, Campbell IL, De Simoni MG, and Vezzani A (2005). Tumor necrosis factor-alpha inhibits seizures in mice via p75 receptors. Ann. Neurol 57, 804–812. [PubMed: 15852477]
40. Bianchi ME (2007). DAMPs, PAMPs and alarmins: all we need to know about danger. J. Leukoc. Biol 81, 1–5.
41. Bezzi P, Domercq M, Brambilla L, Galli R, Schols D, De Clercq E, Vescovi A, Bagetta G, Kollias G, Meldolesi J, and Volterra A (2001). CXCR4-activated astrocyte glutamate release via TNFalpha: amplification by microglia triggers neurotoxicity. Nat. Neurosci 4, 702–710. [PubMed: 11426226]
42. Rojas A, Jiang J, Ganesh T, Yang MS, Lelutiu N, Gueorguieva P, and Dingledine R (2014). Cyclooxygenase-2 in epilepsy. Epilepsia 55, 17–25. [PubMed: 24446952]
43. Xiong ZQ, Qian W, Suzuki K, and McNamara JO (2003). Formation of complement membrane attack complex in mammalian cerebral cortex evokes seizures and neurodegeneration. J. Neurosci 23, 955–960. [PubMed: 12574424]
44. Iori V, Iyer AM, Ravizza T, Beltrame L, Paracchini L, Marchini S, Cerovic M, Hill C, Ferrari M, Zucchetti M, et al. (2017). Blockade of the IL-1R1/TLR4 pathway mediates disease-modification therapeutic effects in a model of acquired epilepsy. Neurobiol. Dis 99, 12–23. [PubMed: 27939857]
45. Somera-Molina KC, Robin B, Somera CA, Anderson C, Stine C, Koh S, Behanna HA, Van Eldik LJ, Watterson DM, and Wainwright MS (2007). Glial activation links early-life seizures and long-term neurologic dysfunction: evidence using a small molecule inhibitor of proinflammatory cytokine upregulation. Epilepsia 48, 1785–1800. [PubMed: 17521344]

46. Abraham J, Fox PD, Condello C, Bartolini A, and Koh S (2012). Minocycline attenuates microglia activation and blocks the long-term epileptogenic effects of early-life seizures. Neurobiol. Dis 46, 425–430. [PubMed: 22366182]
47. Zhao X, Liao Y, Morgan S, Mathur R, Feustel P, Mazurkiewicz J, Qian J, Chang J, Mathern GW, Adamo MA, et al. (2018). Noninflammatory changes of microglia are sufficient to cause epilepsy. Cell Rep. 22, 2080–2093. [PubMed: 29466735]
48. Hwang HW, Saito Y, Park CY, Blachère NE, Tajima Y, Fak JJ, Zucker-Scharff I, and Darnell RB (2017). cTag-PAPERCLIP reveals alternative polyadenylation promotes cell-type specific protein diversity and shifts Araf isoforms with microglia activation. Neuron 95, 1334–1349.e5. [PubMed: 28910620]
49. Zhang B, Zou J, Han L, Beeler B, Friedman JL, Griffin E, Piao YS, Rensing NR, and Wong M (2018). The specificity and role of microglia in epileptogenesis in mouse models of tuberous sclerosis complex. Epilepsia 59, 1796–1806. [PubMed: 30079598]
50. Brand AH, and Perrimon N (1993). Targeted gene-expression as a means ofaltering cell fates and generating dominant phenotypes. Development 118, 401–415. [PubMed: 8223268]
51. Huang DW, Sherman BT, and Lempicki RA (2009). Bioinformatics enrichment tools: paths toward the comprehensive functional analysis of large gene lists. Nucleic Acids Res. 37, 1–13. [PubMed: 19033363]
52. Huang DW, Sherman BT, and Lempicki RA (2009). Systematic and integrative analysis of large gene lists using DAVID bioinformatics resources. Nat. Protoc 4, 44–57. [PubMed: 19131956]
53. Sherman BT, Hao M, Qiu J, Jiao X, Baseler MW, Lane HC, Imamichi T, and Chang W (2022). DAVID: a web server for functional enrichment analysis and functional annotation of gene lists (2021 update). Nucleic Acids Res. 50, W216–W221. [PubMed: 35325185]
54. Panday A, Sahoo MK, Osorio D, and Batra S (2015). NADPH oxidases: an overview from structure to innate immunity-associated pathologies. Cell. Mol. Immunol 12, 5–23. [PubMed: 25263488]
55. Nandi A, Yan LJ, Jana CK, and Das N (2019). Role of catalase in oxidative stress- and age-associated degenerative diseases. Oxid. Med. Cell. Longev 2019, 9613090. [PubMed: 31827713]
56. Barski OA, Tipparaju SM, and Bhatnagar A (2008). The aldo-keto reductase superfamily and its role in drug metabolism and detoxification. Drug Metab. Rev 40, 553–624. [PubMed: 18949601]
57. Hrycay EG, and Bandiera SM (2015). Involvement of cytochrome P450 in reactive oxygen species formation and cancer. Adv. Pharmacol 74, 35–84. [PubMed: 26233903]
58. Ahn SJ, and Marygold SJ (2021). The UDP-glycosyltransferase family in Drosophila melanogaster: nomenclature update, gene expression and phylogenetic analysis. Front. Physiol 12, 648481. [PubMed: 33815151]
59. Whitworth AJ, Theodore DA, Greene JC, Benes H, Wes PD, and Pallanck LJ (2005). Increased glutathione S-transferase activity rescues dopaminergic neuron loss in a Drosophila model of Parkinson's disease. Proc. Natl. Acad. Sci. USA 102, 8024–8029. [PubMed: 15911761]
60. Rada B, and Leto TL (2008). Oxidative innate immune defenses by Nox/Duox family NADPH oxidases. Contrib. Microbiol 15, 164–187. [PubMed: 18511861]
61. DeSalvo MK, Mayer N, Mayer F, and Bainton RJ (2011). Physiologic and anatomic characterization of the brain surface glia barrier of Drosophila. Glia 59, 1322–1340. [PubMed: 21351158]
62. Brown JB, Boley N, Eisman R, May GE, Stoiber MH, Duff MO, Booth BW, Wen J, Park S, Suzuki AM, et al. (2014). Diversity and dynamics of the Drosophila transcriptome. Nature 512, 393–399. [PubMed: 24670639]
63. Hay BA, Wassarman DA, and Rubin GM (1995). Drosophila homologs of baculovirus inhibitor of apoptosis proteins function to block cell death. Cell 83, 1253–1262. [PubMed: 8548811]
64. Wang SL, Hawkins CJ, Yoo SJ, Müller HA, and Hay BA (1999). The Drosophila caspase inhibitor DIAP1 is essential for cell survival and is negatively regulated by HID. Cell 98, 453–63. [PubMed: 10481910]
65. Valanne S, Wang JH, and Rämet M (2011). The Drosophila Toll signaling pathway. J. Immunol 186, 649–656. [PubMed: 21209287]

66. Ip YT, Reach M, Engstrom Y, Kadalayil L, Cai H, González-Crespo S, Tatei K, and Levine M (1993). Dif, a dorsal-related gene that mediates an immune response in Drosophila. Cell 75, 753–763. [PubMed: 8242747]

67. Nicolas E, Reichhart JM, Hoffmann JA, and Lemaitre B (1998). In vivo regulation of the IkappaB homologue cactus during the immune response of Drosophila. J. Biol. Chem 273, 10463–10469. [PubMed: 9553105]

68. Tauszig-Delamasure S, Bilak H, Capovilla M, Hoffmann JA, and Imler JL (2002). Drosophila MyD88 is required for the response to fungal and Gram-positive bacterial infections. Nat. Immunol 3, 91–97. [PubMed: 11743586]

69. Aguiar CCT, Almeida AB, Araújo PVP, de Abreu RNDC, Chaves EMC, do Vale OC, Macêdo DS, Woods DJ, Fonteles MMDF, and Vasconcelos SMM (2012). Oxidative stress and epilepsy: literature review. Oxid. Med. Cell. Longev 2012, 795259. [PubMed: 22848783]

70. Borowicz-Reutt KK, and Czuczwar SJ (2020). Role of oxidative stress in epileptogenesis and potential implications for therapy. Pharmacol. Rep 72, 1218–1226. [PubMed: 32865811]

71. Pauletti A, Terrone G, Shekh-Ahmad T, Salamone A, Ravizza T, Rizzi M, Pastore A, Pascente R, Liang LP, Villa BR, et al. (2019). Targeting oxidative stress improves disease outcomes in a rat model of acquired epilepsy. Brain 142, e39. [PubMed: 31145451]

72. Puttachary S, Sharma S, Stark S, and Thippeswamy T (2015). Seizure-induced oxidative stress in temporal lobe epilepsy. BioMed Res. Int 2015, 745613. [PubMed: 25650148]

73. McElroy PB, Liang LP, Day BJ, and Patel M (2017). Scavenging reactive oxygen species inhibits status epilepticus-induced neuroinflammation. Exp. Neurol 298, 13–22. [PubMed: 28822838]

74. Méndez-Armenta M, Nava-Ruíz C, Juárez-Rebollar D, Rodríguez-Martínez E, and Gómez PY (2014). Oxidative stress associated with neuronal apoptosis in experimental models of epilepsy. Oxid. Med. Cell. Longev 2014, 293689. [PubMed: 25614776]

75. Albrecht SC, Barata AG, Grosshans J, Teleman AA, and Dick TP (2011). In vivo mapping of hydrogen peroxide and oxidized glutathione reveals chemical and regional specificity of redox homeostasis. Cell Metab. 14, 819–829. [PubMed: 22100409]

76. Spindler SR, and Hartenstein V (2010). The Drosophila neural lineages: a model system to study brain development and circuitry. Dev. Genes Evol 220, 1–10. [PubMed: 20306203]

77. Chaplot K, Pimpale L, Ramalingam B, Deivasigamani S, Kamat SS, and Ratnaparkhi GS (2019). SOD1 activity threshold and TOR signalling modulate VAP(P58S) aggregation via reactive oxygen species-induced proteasomal degradation in a Drosophila model of amyotrophic lateral sclerosis. Dis. Model Mech 12, dmm033803. [PubMed: 30635270]

78. Wang Y, Branicky R, Noë A, and Hekimi S (2018). Superoxide dismutases: dual roles in controlling ROS damage and regulating ROS signaling. J. Cell Biol 217, 1915–1928. [PubMed: 29669742]

79. Iori V, Maroso M, Rizzi M, Iyer AM, Vertemara R, Carli M, Agresti A, Antonelli A, Bianchi ME, Aronica E, et al. (2013). Receptor for advanced glycation endproducts is upregulated in temporal lobe epilepsy and contributes to experimental seizures. Neurobiol. Dis 58, 102–114. [PubMed: 23523633]

80. Weinberg MS, Blake BL, and McCown TJ (2013). Opposing actions of hippocampus TNFalpha receptors on limbic seizure susceptibility. Exp. Neurol 247, 429–437. [PubMed: 23333565]

81. Bulet P, Uttenweiler-Joseph S, Moniatte M, Van Dorsselaer A, and Hoffmann JA (1998). Differential display of peptides induced during the immune response of Drosophila: a matrix-assisted laser desorption ionization time-of-flight mass spectrometry study. J. Protein Chem 17, 528–529.

82. Imler JL, Ferrandon D, Royet J, Reichhart JM, Hetru C, and Hoffmann JA (2004). Toll-dependent and Toll-independent immune responses in Drosophila. J. Endotoxin Res 10, 241–246. [PubMed: 15373968]

83. Lemaitre B, Nicolas E, Michaut L, Reichhart JM, and Hoffmann JA (1996). The dorsoventral regulatory gene cassette spatzle/Toll/cactus controls the potent antifungal response in Drosophila adults. Cell 86, 973–983. [PubMed: 8808632]

84. Tanji T, Yun EY, and Ip YT (2010). Heterodimers of NF-kappaB transcription factors DIF and Relish regulate antimicrobial peptide genes in Drosophila. Proc. Natl. Acad. Sci. USA 707, 14715–14720.

85. Guo C, Sun L, Chen X, and Zhang D (2013). Oxidative stress, mitochondrial damage and neurodegenerative diseases. Neural Regen. Res 8, 2003–2014. [PubMed: 25206509]

86. Salminen TS, and Vale PF (2020). Drosophila as a model system to investigate the effects of mitochondrial variation on innate immunity. Front. Immunol 11, 521. [PubMed: 32269576]

87. Blaser H, Dostert C, Mak TW, and Brenner D (2016). TNF and ROS crosstalk in inflammation. Trends Cell Biol. 26, 249–261. [PubMed: 26791157]

88. West AP, and Shadel GS (2017). Mitochondrial DNA in innate immune responses and inflammatory pathology. Nat. Rev. Immunol 17, 363–375. [PubMed: 28393922]

89. Uddin MS, Hasana S, Ahmad J, Hossain MF, Rahman MM, Behl T, Rauf A, Ahmad A, Hafeez A, Perveen A, and Ashraf GM (2021). Anti-neuroinflammatory potential of polyphenols by inhibiting NF-kappaB to halt Alzheimer's disease. Curr. Pharm. Des 27, 402–414. [PubMed: 33213314]

90. Buchon N, Silverman N, and Cherry S (2014). Immunity in Drosophila melanogaster–from microbial recognition to whole-organism physiology. Nat. Rev. Immunol 14, 796–810. [PubMed: 25421701]

91. Guo W, Stoklund Dittlau K, and Van Den Bosch L (2020). Axonal transport defects and neurodegeneration: molecular mechanisms and therapeutic implications. Semin. Cell Dev. Biol 99, 133–150. [PubMed: 31542222]

92. Shidara Y, and Hollenbeck PJ (2010). Defects in mitochondrial axonal transport and membrane potential without increased reactive oxygen species production in a Drosophila model of Friedreich ataxia. J. Neurosci 30, 11369–11378. [PubMed: 20739558]

93. Liao PC, Tandarich LC, and Hollenbeck PJ (2017). ROS regulation of axonal mitochondrial transport is mediated by Ca2+ and JNK in Drosophila. PLoS One 12, e0178105. [PubMed: 28542430]

94. Swanson LC, Rimkus SA, Ganetzky B, and Wassarman DA (2020). Loss of the antimicrobial peptide Metchnikowin protects against traumatic brain injury outcomes in Drosophila melanogaster. G3 10, 3109–3119. [PubMed: 32631949]

95. Cao Y, Chtarbanova S, Petersen AJ, and Ganetzky B (2013). Dnr1 mutations cause neurodegeneration in Drosophila by activating the innate immune response in the brain. Proc. Natl. Acad. Sci. USA 110, E1752–E1760. [PubMed: 23613578]

96. Badinloo M, Nguyen E, Suh W, Alzahrani F, Castellanos J, Klichko VI, Orr WC, and Radyuk SN (2018). Overexpression of antimicrobial peptides contributes to aging through cytotoxic effects in Drosophila tissues. Arch. Insect Biochem. Physiol 98, e21464. [PubMed: 29637607]

97. Imler JL, and Bulet P (2005). Antimicrobial peptides in Drosophila: structures, activities and gene regulation. Chem. Immunol. Allergy 86, 1–21. [PubMed: 15976485]

98. Ageitos JM, Sánchez-Pérez A, Calo-Mata P, and Villa TG (2017). Antimicrobial peptides (AMPs): ancient compounds that represent novel weapons in the fight against bacteria. Biochem. Pharmacol 133, 117–138. [PubMed: 27663838]

99. Stuart BAR, and Franitza AL (2022). Regulatory roles of antimicrobial peptides in the nervous system: implications for neuronal aging. Front. Cell. Neurosci 16, 843790. [PubMed: 35321204]

100. Liddelow SA, Guttenplan KA, Clarke LE, Bennett FC, Bohlen CJ, Schirmer L, Bennett ML, Münch AE, Chung WS, Peterson TC, et al. (2017). Neurotoxic reactive astrocytes are induced by activated microglia. Nature 541, 481–487. [PubMed: 28099414]

101. Mortensen SA, Sander B, Jensen RK, Pedersen JS, Golas MM, Jensenius JC, Hansen AG, Thiel S, and Andersen GR (2017). Structure and activation of C1, the complex initiating the classical pathway of the complement cascade. Proc. Natl. Acad. Sci. USA 114, 986–991. [PubMed: 28104818]

102. Schneider CA, Rasband WS, and Eliceiri KW (2012). NIH Image to ImageJ: 25 years of image analysis. Nat. Methods 9, 671–675. [PubMed: 22930834]

103. Gevedon O, Bolus H, Lye SH, Schmitz K, Fuentes-Gonzalez J, Hatchell K, Bley L, Pienaar J, Loewen C, and Chtarbanova S (2019). In vivo forward genetic screen to identify novel neuroprotective genes in Drosophila melanogaster. J. Vis. Exp 10.3791/59720.

104. Pinsonneault RL, Mayer N, Mayer F, Tegegn N, and Bainton RJ (2011). Novel models for studying the blood-brain and blood-eye barriers in Drosophila. Methods Mol. Biol 686, 357–369. [PubMed: 21082381]

105. Santana JF, Parida M, Long A, Wankum J, Lilienthal AJ, Nukala KM, and Manak JR (2020). The Dm-Myb oncoprotein contributes to insulator function and stabilizes repressive H3K27me3 PcG domains. Cell Rep. 30, 3218–3228.e5. [PubMed: 32160531]

106. Hu Y, Sopko R, Foos M, Kelley C, Flockhart I, Ammeux N, Wang X, Perkins L, Perrimon N, and Mohr SE (2013). FlyPrimerBank: an online database for Drosophila melanogaster gene expression analysis and knockdown evaluation of RNAi reagents. G3 3, 1607–1616. [PubMed: 23893746]

Highlights

- *pk*^{sple} neurons show increased oxidative stress that activates the glial immune system
- Glial innate immune response promotes neuronal cell death
- Increased cell death coupled with glial activation creates a positive feedback loop
- Increased neuronal cell death leads to progression of seizure phenotype

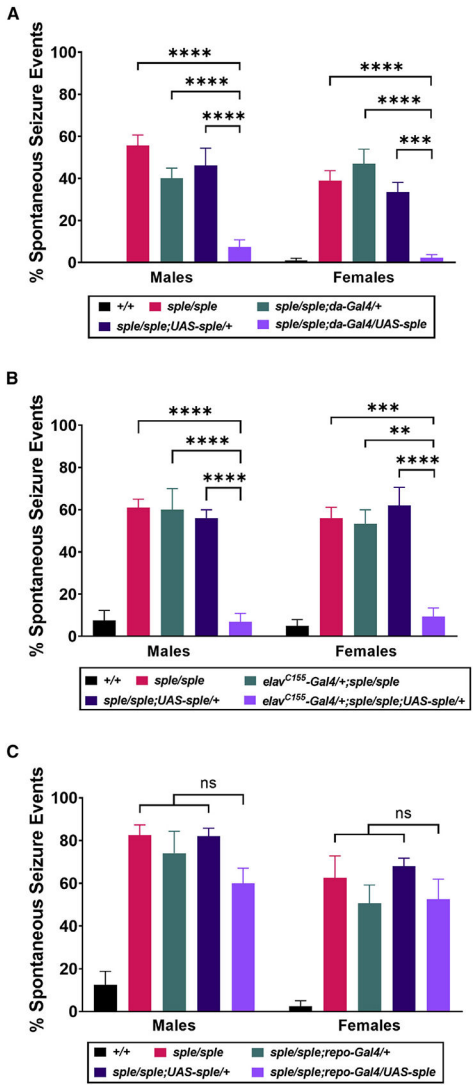

Figure 1. Expressing *pk*^{sple} in neurons, but not glia, is sufficient to suppress seizures in homozygous *pk*^{sple} mutants

(A) Spontaneous seizure quantification in 15 dpe males and females of indicated genotypes reveals significant reduction in seizures when *pk*^{sple} is expressed ubiquitously. n = 5–8/genotype.

(B) Spontaneous seizure quantification in 15 dpe males and females of indicated genotypes reveals significant reduction in seizures when *pk*^{sple} is expressed pan-neuronally. n = 3–5/genotype.

(C) Spontaneous seizure quantification in 15 dpe males and females of indicated genotypes reveals no significant reduction in seizures when *pk*^{sple} is expressed in glial cells. n = 4–5/genotype.

Data are shown as mean ± SEM; one-way ANOVA with Holm-Sidak multiple comparisons test. n = number of seizure assays performed, 8–10 flies/assay. **p ≤ 0.01, ***p ≤ 0.001, ****p ≤ 0.0001. ns, no significant difference. For source data, see Data S3.

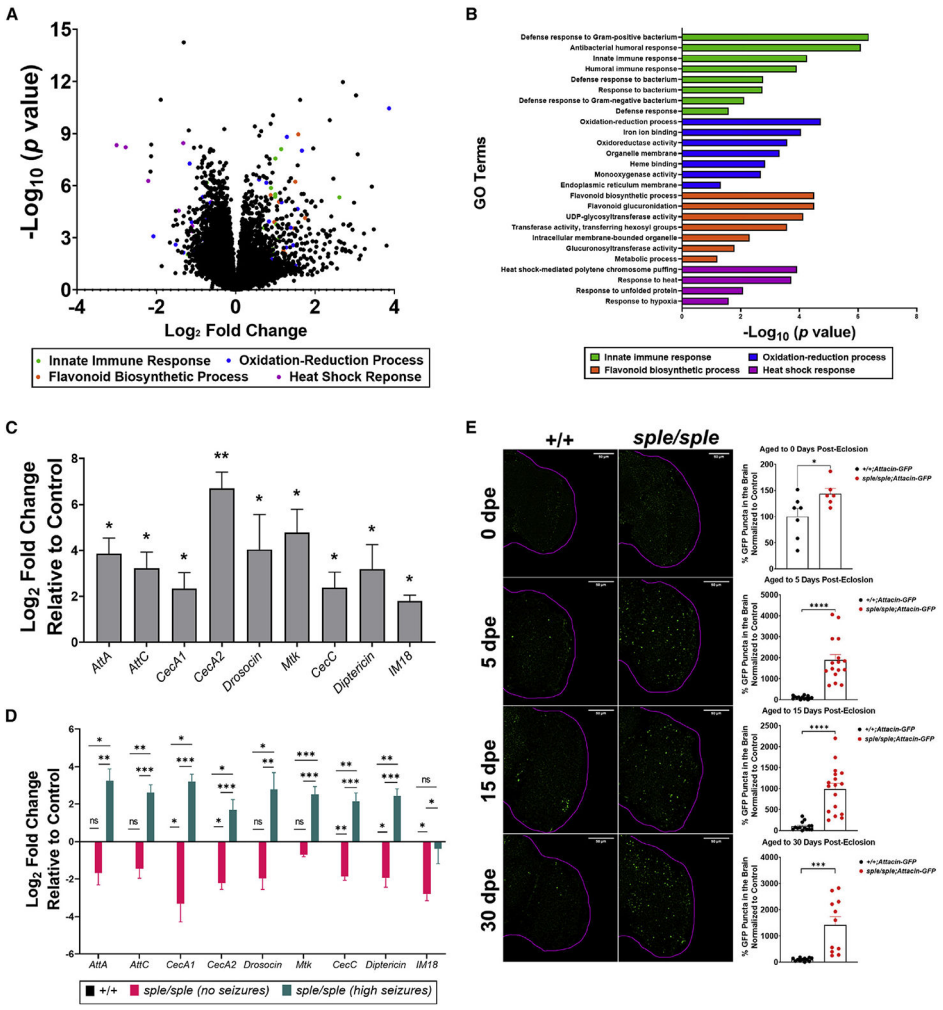

Figure 2. *pk*^{sple} mutant brains show significant upregulation of innate immune response pathway genes across adulthood

(A) Volcano plot of microarray analysis of 7–10 dpe *sple/sple* brains compared with controls. $\log_{10}$ p values (y axis) were plotted against $\log_2$ fold changes (x axis); $p < 0.05$ and fold changes of ≤0.66 and ≥ 1.5 were used to call genes as being significantly downregulated or upregulated, respectively. Top Gene Ontology categories: innate immune response (green), oxidation-reduction process (blue), flavonoid biosynthesis process (orange), and heat shock response (magenta).

(B) Gene Ontology terms based on enrichment scores (as in A) are listed in descending order: innate immune response, oxidation-reduction process, flavonoid biosynthetic process, and heat shock response.

(C) qRT-PCR of 7–10 dpe *sple/sple* brains showing $\log_2$ fold-change values of specific AMP genes relative to control. All AMP genes show significant increase in expression in *sple/sple* brains. Data are shown as mean ± SEM; Student's t test. n = 3 biological replicates/genotype.

(D) qRT-PCR of 7–10 dpe control, *sple/sple* brains from flies with no seizure penetrance, and *sple/sple* brains from flies with high seizure penetrance. Most AMPs show significantly higher expression in *sple/sple* mutants with high seizures compared with control or *sple/sple*

mutants that had no seizures, whereas the level of expression of AMP genes was either unchanged or significantly lower in *sple/sple* mutants with no seizures relative to control. Data are shown as mean ± SEM; one-way ANOVA with Tukey's multiple comparisons test. n = 3 biological replicates/group.

(E) Representative confocal images and quantification of *Attacin*-GFP puncta (shown in green) normalized to controls in both +/+ and *sple/sple* mutant brains aged to 0, 5, 15, and 30 dpe show significant increase in *Attacin*-GFP puncta in *sple/sple* brains for all time points. Data shown are mean ± SEM; Student's t test. Dots represent individual values. n = 6–17 brains/genotype. Scale bars, 50 μm.

*p ≤ 0.05, **p ≤ 0.01, ***p ≤ 0.001, ****p ≤ 0.0001. For source data, see Data S3.

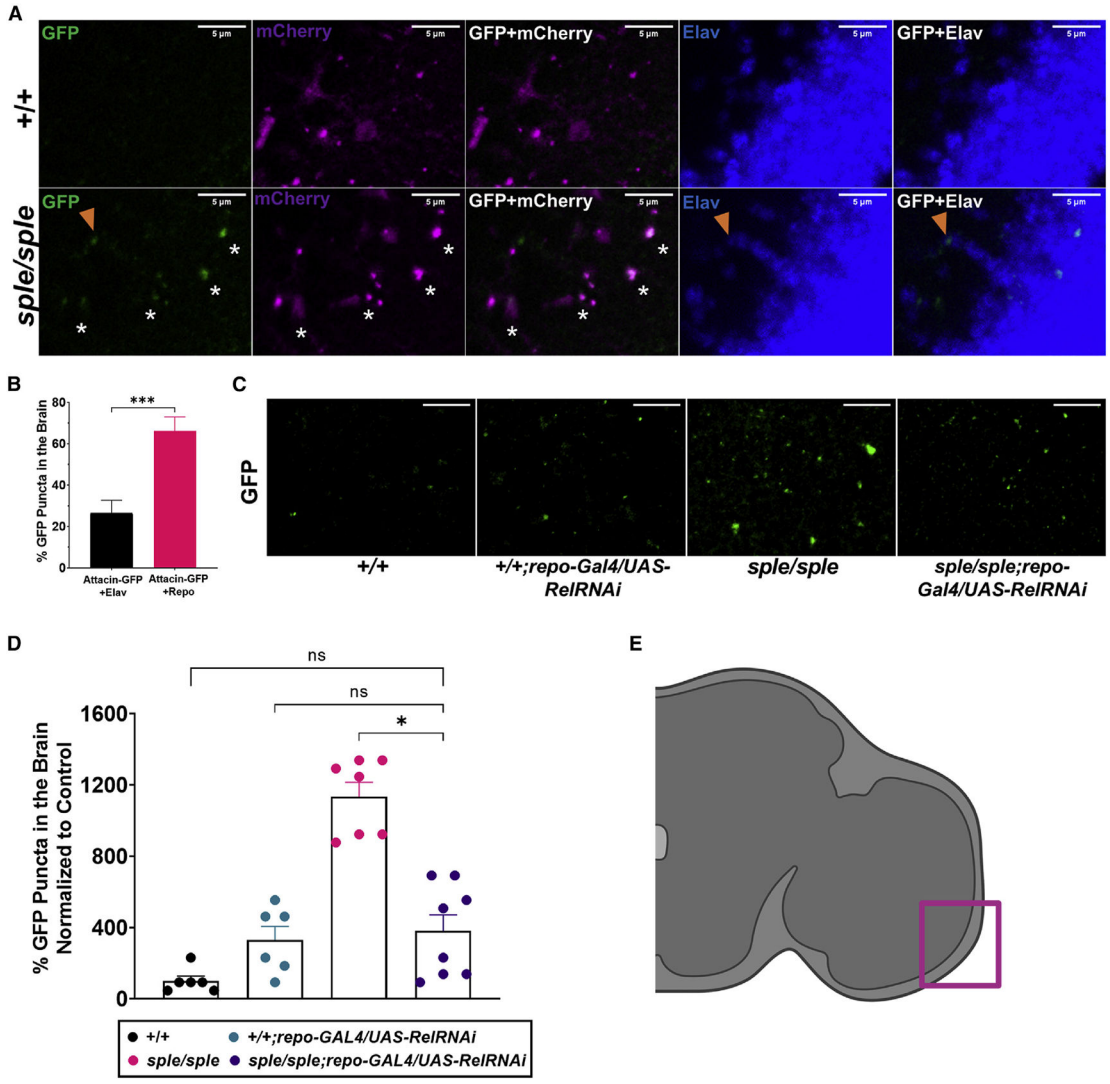

Figure 3. Glial cells are the source of AMP expression in pk^{sple} mutant brains

(A) Representative confocal images of 15 dpe *+/+;Attacin-GFP* and *sple/sple;Attacin-GFP* optic lobes expressing mCherry in glia using *repo-Gal4* driver and immunostained for GFP (green), mCherry (magenta), and neuronal marker Elav (blue). Colocalization of GFP with mCherry is indicated by white asterisks, whereas colocalization of GFP with Elav is indicated by orange arrowheads. Scale bars, 5 μm.

(B) Quantification of percentage of Attacin-GFP puncta colocalizing with either Elav or mCherry reveals that most puncta overlap with mCherry (glia) in *sple/sple* brains. Data are shown as mean ± SEM; Mann-Whitney test. n = 19 confocal sections/group.

(C) Representative confocal images of optic lobe regions of +/+, *+/+;repo-Gal4/UAS-RelRNAi*, *sple/sple*, and *sple/sple;repo-Gal4/UAS-RelRNAi* expressing *Attacin*-GFP and immunostained for GFP in green. A decrease in GFP staining is observed in the brains of *sple/sple* mutants when *Relish* is knocked down specifically in glia. Scale bars, 20 μm.

(D) Quantification of *Attacin*-GFP puncta normalized to control in +/+, *+/+;repo-Gal4/UAS-RelRNAi, sple/sple*, and *sple/sple;repo-Gal4/UAS-RelRNAi* shows significant decrease in

Attacin-GFP puncta in *sple/sple* brains when *Relish* is knocked down specifically in glia. Data are shown as mean ± SEM; Kruskal-Wallis with Dunn's multiple comparison test. Dots represent individual values. n = 6–8 brains/genotype.

(E) Schematic diagram of a *Drosophila* brain highlighting the region (magenta box) used for obtaining representative confocal images shown in (A) and (C).

*p ≤ 0.05, ***p ≤ 0.001. For source data, see Data S3.

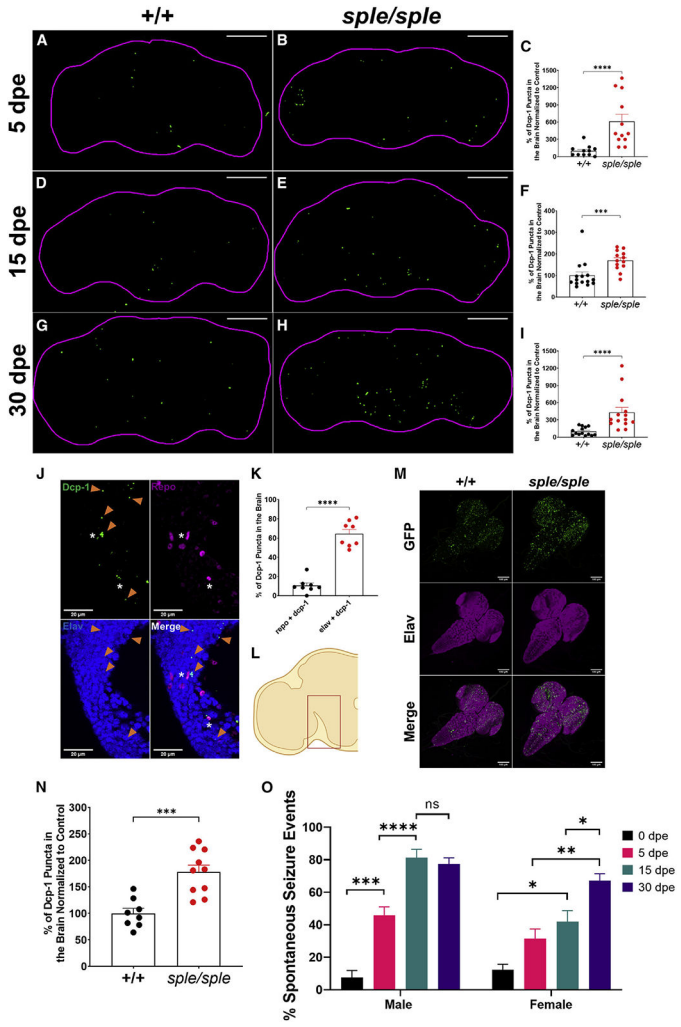

Figure 4. *pk*^{sple} mutants have sustained neuronal cell death and exacerbation of seizures with age

(A and B) Representative confocal images of 5 dpe +/+ (A) and *sple/sple* (B) adult brains stained for apoptosis marker Dcp-1 (green). Scale bars, 100 μm.

(C) Quantification of Dcp-1 puncta in (A) and (B) normalized to 5 dpe controls reveals significant increase in neuronal cell death in *sple/sple* brains. Data are shown as mean ± SEM; Mann-Whitney test. Dots represent individual values. n = 11–12 brains/genotype.

(D and E) Representative confocal images of 15 dpe +/+ (D) and *sple/sple* (E) brains stained for Dcp-1 (green). Scale bars, 100 μm.

(F) Quantification of Dcp-1 puncta in (D) and (E) normalized to 15 dpe controls reveals significant increase in neuronal cell death in *sple/sple* brains. Data are shown as mean ± SEM; Mann-Whitney test. Dots represent individual values. n = 13–15 brains/genotype

(G and H) Representative confocal images of 30 dpe +/+ (G) and *sple/sple* (H) brains stained for Dcp-1 (green). Scale bars, 100 μm.

(I) Quantification of Dcp-1 puncta in (G) and (H) normalized to 30 dpe controls reveals significant increase in neuronal cell death in *sple/sple* brains. Data are shown as mean ± SEM; Mann-Whitney test. Dots represent individual values. n = 14 brains/genotype.

(J) Representative confocal images of 15 dpe *sple/sple* brains immunostained for Dcp-1 (green), glial marker Repo (magenta), and neuronal marker Elav (blue). Colocalization of Dcp-1 puncta with Repo and Elav is indicated by white asterisks and orange arrowheads, respectively. Scale bars, 20 μm.

(K) Quantification of percentage of Dcp-1 puncta in *sple/sple* brains colocalizing with either Repo or Elav. A significantly higher percentage of Dcp-1 puncta colocalize with Elav. Data are shown as mean ± SEM; Student's t test. Dots represent individual values. n = 8 brains/group.

(L) Schematic diagram of *Drosophila* brain highlighting the region (red box) used for obtaining representative confocal images in (J).

(M) Representative confocal images of third instar larval brains of +/+ and *sple/sple* mutants stained for Dcp-1 in green, Elav in magenta, and merged image of Dcp-1 and Elav. Scale bars, 100 μm.

(N) Quantification of Dcp-1 puncta in third instar larval brains normalized to controls shows significant increase in neuronal cell death in *sple/sple* larval brains. Data are shown as mean ± SEM; Student's t test. Dots represent individual values. n = 8–10 brains/genotype.

(O) Quantification of spontaneous seizures in males and females of *sple/sple* mutants aged to 0, 5, 15, and 30 dpe. Both male and female *sple/sple* mutants show an increase in spontaneous seizures across adulthood.

Data are shown as mean ± SEM; one-way ANOVA with Tukey's multiple comparisons test. n = 3–9 seizure assays/group, 8–10 flies/assay. *p ≤ 0.05, **p ≤ 0.01, ***p ≤ 0.001, ****p ≤ 0.0001. For source data, see Data S3.

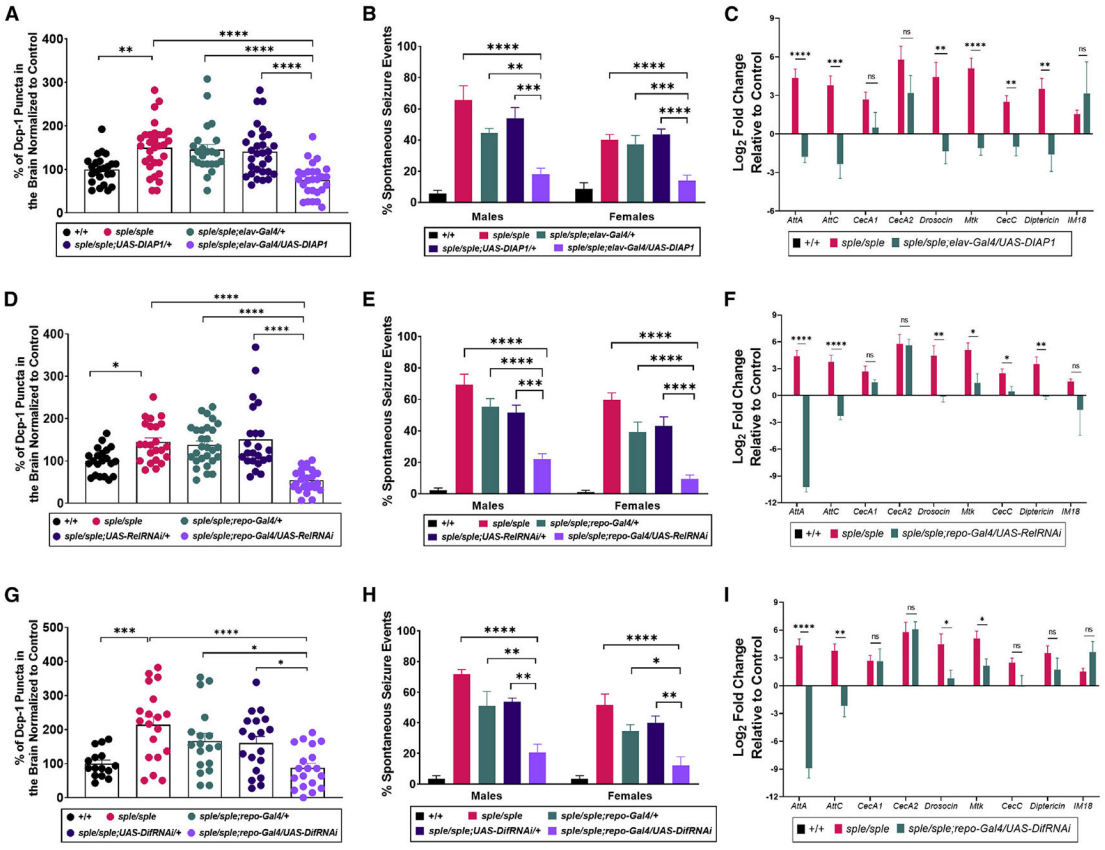

Figure 5. Inhibition of glial IIR in *pk*^{sple} mutants leads to significant suppression of neuronal cell death, which in turn suppresses seizure exacerbation

(A) Quantification of Dcp-1 puncta in brains normalized to controls (+/+) reveals significant suppression in neuronal cell death in *sple/sple;elav-Gal4/UAS-DIAP1* brains when compared with *sple/sple, sple/sple;elav-Gal4/+*, and *sple/sple;UAS-DIAP1/+. sple/sple* mutant brains also show significant increase in Dcp-1 puncta when compared with +/+. Data are shown as mean ± SEM; Kruskal-Wallis with Dunn's multiple comparisons test. Dots represent individual values. n = 23–31 brains/genotype.

(B) Quantification of spontaneous seizures in 15 dpe males and females of indicated genotypes reveals significant reduction in spontaneous seizures when *DIAP1* is overexpressed specifically in neurons of *sple/sple* mutants. Data are shown as mean ± SEM; one-way ANOVA with Dunnett's multiple comparisons test. n = 5–12 seizure assays/group, 8–10 flies/assay.

(C) qRT-PCR of 7–10 dpe +/+, *sple/sple*, and *sple/sple;elav-Gal4/UAS-DIAP1* mutant brains showing $\log_2$ fold-change values of specific AMP genes relative to control. Most AMP genes show significant downregulation in *sple/sple;elav-Gal4/UAS-DIAP1* brains relative to *sple/sple* brains. Data are shown as mean ± SEM; one-way ANOVA test with Tukey's multiple comparisons test. n = 4 biological replicates/genotype.

(D) Quantification of Dcp-1 puncta in brains normalized to controls (+/+) reveals significant suppression in neuronal cell death in *sple/sple;repo-Gal4/UAS-RelRNAi* brains when compared with *sple/sple, sple/sple;repo-Gal4/+*, and *sple/sple;UAS-RelRNAi/+. sple/sple* mutant brains also show significant increase in Dcp-1 puncta when compared with +/+. Data

are shown as mean ± SEM; Kruskal-Wallis with Dunn's multiple comparisons test. Dots represent individual values. n = 21–28 brains/genotype.

(E) Quantification of spontaneous seizures in 15 dpe males and females of +/+, *sple/sple, sple/sple;repo-Gal4/+, sple/sple;UAS-RelRNAi/+*, and *sple/sple;repo-Gal4/UAS-RelRNAi* shows significant reduction in spontaneous seizures when *Relish* is knocked down specifically in glia. Data are shown as mean ± SEM; one-way ANOVA with Dunnett's multiple comparisons test. n = 8–11 seizure assays/group, 8–10 flies/assay.

(F) qRT-PCR of 7–10 dpe +/+, *sple/sple*, and *sple/sple;repo-Gal4/UAS-RelRNAi* mutant brains showing $\log_2$ fold-change values of specific AMP genes relative to control. Most AMP genes show significant downregulation in *sple/sple;repo-Gal4/UAS-RelRNAi* brains relative to *sple/sple* mutant brains. Data are shown as mean ± SEM; one-way ANOVA test with Tukey's multiple comparisons test. n = 4 biological replicates/genotype.

(G) Quantification of Dcp-1 puncta in brains normalized to controls (+/+) reveals significant suppression in neuronal cell death in *sple/sple;repo-Gal4/UAS-DifRNAi* brains when compared with *sple/sple, sple/sple;repo-Gal4/+*, and *sple/sple;UAS-DifRNAi/+. sple/sple* brains also show significant increase in Dcp-1 puncta when compared with +/+. Data are shown as mean ± SEM; one-way ANOVA with Dunnett's multiple comparisons test. Dots represent individual values. n = 15–19 brains/genotype.

(H) Quantification of spontaneous seizures in 15 dpe males and females of +/+, *sple/sple, sple/sple;repo-Gal4/+, sple/sple;UAS-DifRNAi/+*, and *sple/sple;repo-Gal4/UAS-DifRNAi* reveals significant reduction in spontaneous seizures when *Dif* is knocked down specifically in glia. Data are shown as mean ± SEM; one-way ANOVA with Dunnett's multiple comparisons test. n = 5–7 seizure assays/group, 8–10 flies/assay.

(I) qRT-PCR of 7–10 dpe +/+, *sple/sple*, and *sple/sple;repo-Gal4/UAS-DifRNAi* mutant brains showing $\log_2$ fold-change values of specific AMP genes relative to control. Four AMP genes show significant downregulation in *sple/sple;repo-Gal4/UAS-DifRNAi* brains relative to *sple/sple* brains.

Data are shown as mean ± SEM; one-way ANOVA test with Tukey's multiple comparisons test. n = 4 biological replicates/genotype. *p ≤ 0.05, **p ≤ 0.01, ***p ≤ 0.001, ****p ≤ 0.0001. See Figure S5 for representative images. For source data, see Data S3.

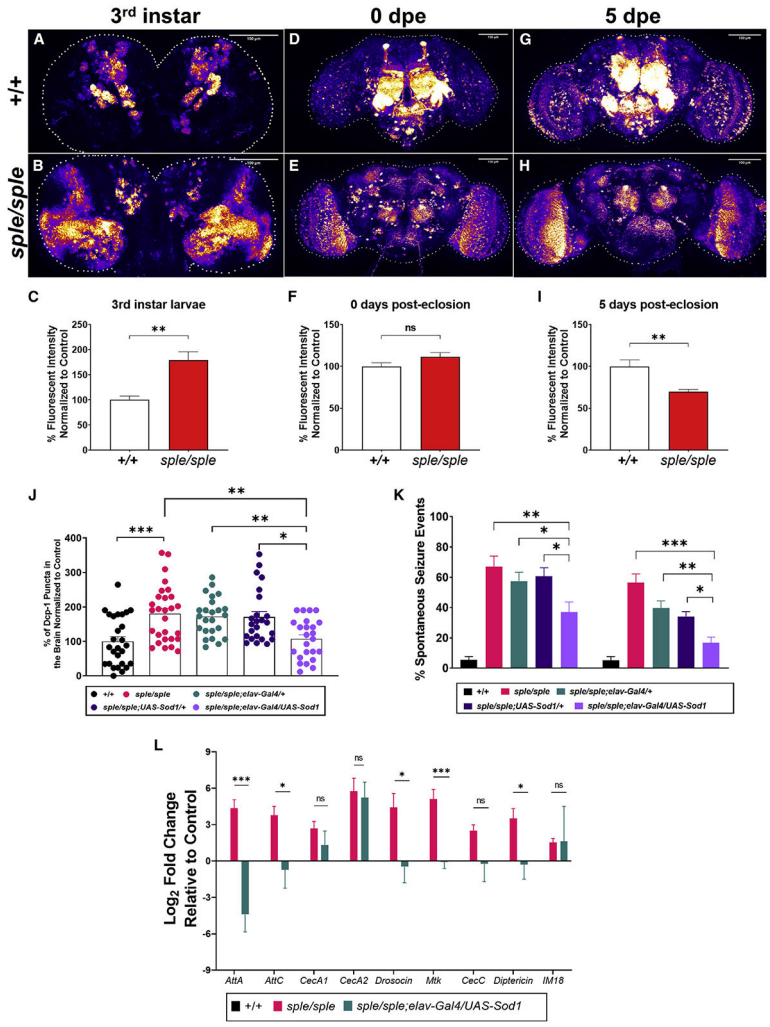

Figure 6. *pk*^{sple} mutant brains show increased neuronal oxidative stress that contributes to an increase in innate immune response, neuronal cell death, and seizure progression

(A and B) Representative confocal live images of +/+ (A) and *sple/sple* (B) larval brains expressing mitochondrial ROS GFP reporter (mt-roGFP2-Orp1).

(C) Quantification of mitochondrial ROS-activated fluorescent intensity normalized to control reveals significant increase in fluorescent intensity in *sple/sple* larval brains.

(D and E) Representative confocal live images of 0 dpe +/+ (D) and *sple/sple* (E) adult brains expressing mitochondrial ROS GFP reporter.

(F) Quantification of mitochondrial ROS-activated fluorescent intensity normalized to control reveals no significant increase in overall fluorescent intensity in 0 dpe *sple/sple* brains.

(G and H) Representative confocal live images of 5 dpe +/+ (G) and *sple/sple* (H) adult brains expressing mitochondrial ROS GFP reporter.

(I) Quantification of mitochondrial ROS-activated fluorescent intensity normalized to control reveals significant decrease in fluorescent intensity in 5 dpe *sple/sple* brains. For (C), (F), and (I), data are shown as mean ± SEM; Student's t test. n = 4–8 brains/genotype. **p ≤ 0.01. Scale bars, 100 μm.

(J) Quantification of Dcp-1 puncta in brains normalized to controls (+/+) shows significant suppression in neuronal cell death in *sple/sple;elav-Gal4/UAS-Sod1* brains when compared with *sple/sple, sple/sple;elav-Gal4/+*, and *sple/sple;UAS-Sod1/+. sple/sple* brains also show a significant increase in Dcp-1 puncta when compared with +/+. Data are shown as mean ± SEM; Kruskal-Wallis with Dunn's multiple comparisons test. Dots represent individual values. n = 24–28 brains/genotype. See Figure S6 for representative images.
(K) Quantification of spontaneous seizures in 15 dpe males and females of indicated genotypes shows significant reduction in spontaneous seizures when *Sod1* is overexpressed specifically in neurons of *sple/sple* mutants. Data are shown as mean ± SEM; one-way ANOVA with Dunnett's multiple comparisons test. n = 5–9 seizure assays/group, 8–10 flies/assay.
(L) qRT-PCR of 7–10 dpe +/+, *sple/sple*, and *sple/sple;elav-Gal4/UAS-Sod1* mutant brains showing $\log_2$ fold-change values of specific AMP genes relative to control. Most AMP genes show significant downregulation in *sple/sple;elav-Gal4/UAS-Sod1* brains relative to *sple/sple* brains. Data are shown as mean ± SEM; one-way ANOVA test with Tukey's multiple comparisons test. n = 4 biological replicates/genotype.
For source data, see Data S3.

KEY RESOURCES TABLE

REAGENT or RESOURCE	SOURCE	IDENTIFIER
Antibodies		
Rabbit anti-Dcp1	Cell Signaling Technologies	Cat#9578; RRID: AB_2721060
Rat anti-Elav	DSHB	Cat#7E8A10; RRID: AB_528218
Mouse anti-repo	DSHB	Cat#8D12; RRID: AB_528448
Rabbit anti-GFP	Invitrogen	Cat#A-11122; RRID: AB_221569
Mouse anti-mCherry	DSHB	Cat#3A11; RRID: AB_2617430
Alexa Flour 488-conjugated goat anti-rabbit	Invitrogen	Cat#A-11008; RRID: AB_143165
Alexa Flour 568-conjugated goat anti-mouse	Invitrogen	Cat#A-11004; RRID: AB_2534072
Alexa Flour 568-conjugated goat anti-rat	Invitrogen	Cat#A-11077; RRID: AB_2534121
Alexa Flour 633-conjugated goat anti-rat	Invitrogen	Cat#A-21094; RRID: AB_2535749
Vectashield	Vector Laboratories	Cat#H-1000; RRID: AB_2336789
Alexa Flour 488-Dextran 10,000 MW	Invitrogen	Cat#D2291
Critical commercial assays		
RNAqueous-Micro Total RNA Isolation kit	Invitrogen	Cat#AM1931
High-Capacity RNA to cDNA kit	Applied Biosystems	Cat#4387406
PowerUp SYBR Green Master Mix	Applied Biosystems	Cat#A25742
Deposited data		
Raw and Analyzed data	This paper	GEO: GSE154686
Experimental models: Organisms/strains		
w^{1118}	Gift from Andy Frank	N/A
pk^{sple-1}	Bloomington Drosophila Stock Center	RRID: BDSC_422
Rel^{E20}	Bloomington Drosophila Stock Center	RRID: BDSC_55714
UAS-Relish-RNAi	Bloomington Drosophila Stock Center	RRID: BDSC_33661
UAS-Dif-RNAi	Bloomington Drosophila Stock Center	RRID: BDSC_30513
repo-GAL4	Bloomington Drosophila Stock Center	RRID: BDSC_7415
elav-GAL4	Bloomington Drosophila Stock Center	RRID: BDSC_8760
$elav^{C155}$*-GAL4*	Bloomington Drosophila Stock Center	RRID: BDSC_33805
da-GAL4	Gift from Toshihiro Kitamoto	N/A
UAS-DIAP1	Bloomington Drosophila Stock Center	RRID: BDSC_6657
UAS-mito-roGFP2-Orp1	Bloomington Drosophila Stock Center	RRID: BDSC_67667
UAS-Sod1	Bloomington Drosophila Stock Center	RRID: BDSC_24750

REAGENT or RESOURCE	SOURCE	IDENTIFIER
moody^{attP}	Bloomington Drosophila Stock Center	RRID: BDSC_84522
Attacin-GFP	Gift from David Wassarman	N/A
Cecropin-GFP	Gift from David Wassarman	N/A
Drosocin-GFP	Gift from David Wassarman	N/A
Oligonucleotides		
Primers for quantitative real-time PCR, see Table S1	This paper	N/A
Software and algorithms		
ArrayStar (Version 12.0.0)	DNASTAR, Inc.	https://www.dnastar.com/
Graphpad Prism 9	Graphpad Software	https://www.graphpad.com/scientific-software/prism/; RRID: SCR_002798
DAVID	Sherman et al.[53] and Huang et al.[52]	https://david.ncifcrf.gov/; RRID: SCR_001881
ImageJ	Schneider et al.[102]	https://imagej.nih.gov/ij/; RRID: SCR_003070
Leica SP5 confocal microscope	Leica	https://www.leica-microsystems.com/products/confocal-microscopes/p/leica-tcs-sp5/; RRID: SCR_002140
Leica SP8 confocal microscope	Leica	https://www.leica-microsystems.com/products/confocal-microscopes/p/leica-tcs-sp8/; RRID: SCR_018169
Nikon Eclipse E100 light microscope	Nikon	https://www.microscope.healthcare.nikon.com/products/upright-microscopes/eclipse-e100
Adobe Creative Cloud Photoshop	Adobe	https://www.adobe.com/products/photoshop.html; RRID: SCR_014199
Design and Analysis Software Version 2.6, QuantStudio 6/7 Pro systems	Applied Biosystems	https://www.thermofisher.com/us/en/home/global/forms/life-science/quantstudio-6-7-pro-software.html
Applied Biosystems 7900HT Fast Real-Time PCR system	Applied Biosystems	https://www.thermofisher.com/order/catalog/product/4351405#/4351408; RRID: SCR_018060